

An investigation of fixed separation in quasi-periodic and aperiodic, unsteady, two-dimensional flows

by

Moneer Mohammad Helu

Submitted to the Department of Mechanical Engineering
in partial fulfillment of the requirements for the degree of

Bachelor of Science

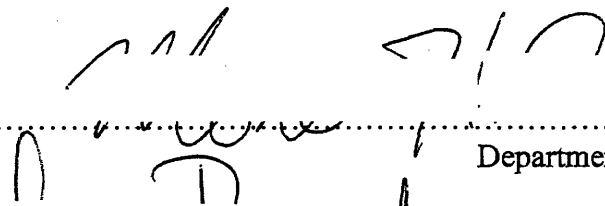
at the

MASSACHUSETTS INSTITUTE OF TECHNOLOGY

June 2007

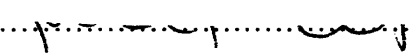
© 2007 Massachusetts Institute of Technology. All rights reserved.

Signature of Author.....



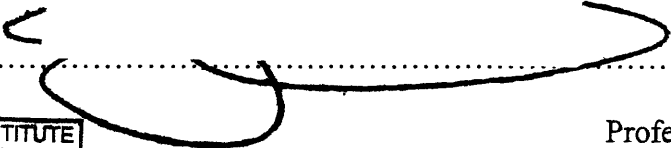
Department of Mechanical Engineering
11 May 2007

Certified by.....

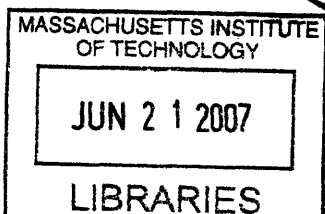


Thomas Peacock
ARCO Assistant Professor of Mechanical Engineering
Thesis Supervisor

Accepted by.....



John H. Lienhard V
Professor of Mechanical Engineering
Chairman, Undergraduate Thesis Committee



ARCHIVES

An investigation of fixed separation in quasi-periodic and aperiodic, unsteady, two-dimensional flows

by

Moneer Mohammad Helu

Submitted to the Department of Mechanical Engineering
on 11 May 2007, in partial fulfillment of the
requirements for the degree of
Bachelor of Science in Mechanical Engineering

ABSTRACT

This study assesses the kinematic theory of fixed separation in unsteady, two-dimensional flows that has been proposed by Haller (2004). Experimental investigations were conducted that utilized the rotor-oscillator flow to drive low Reynolds number quasi-periodic and aperiodic flows. Flow separation was observed using flow visualization techniques that employed fluorescent dye. These experimental investigations show the existence of fixed separation in both quasi-periodic and aperiodic flows. The experimental results also suggest that the location of fixed separation is immune to relatively quick variations in the flow. Thus, the 'typical' behavior of a quasi-periodic or aperiodic flow dictates the location of fixed separation in addition to the amplitude of oscillation of the flow. Both of these findings imply that the time averaged zero skin friction point is a stronger predictor of separation, which supports the Haller (2004) criteria. Furthermore, while still premature, the experimental results have so far been corroborated by early numerical simulations of the Haller (2004) criteria in the quasi-periodic flows investigated in this study.

Thesis Supervisor: Thomas Peacock

Title: ARCO Associate Professor of Mechanical Engineering

Acknowledgements

First and foremost, I must thank my advisor, Professor Thomas Peacock. Thank you so much for allowing me to work in your lab, for the advice and guidance you always had whenever I needed it, for your dedication to and respect for your students, for the enthusiasm you have always shown towards the research, and most of all for your continued support, encouragement, and patience throughout the duration of this project. Even though I was only a sophomore, you took a chance on me and gave me ownership of a project. After two years, I have learned so much about myself and about the subject material. I will always be grateful for the opportunities you have given me.

I also must express my appreciation to the many other people who have helped me throughout this project. To Andy Gallant, thank you so much for helping me design and build the different modules I always needed for the experimental apparatus. To Andy Watchorn, thank you for spending several afternoons with me as I tried to debug my LabView wiring diagrams. To Guus Jacobs, thank you for your help on the numerical analysis and for coming up several times my first summer to help me through problems with the apparatus. To Steve Reece, thank you for teaching me how to use the laser equipment and helping me set up all the optics. Lastly, I must thank the other members of the Nonlinear Dynamics Lab, especially Matt Weldon. Thank you so much Matt for always helping me whenever I needed it, for letting me work with you this past year, and most of all, for all the advice and guidance you have given me. I truly appreciate it all.

Finally, there are many people outside of work and research who I would be remiss for not acknowledging. I must thank all my friends for their continued support and encouragement throughout this process, especially Rabia. To Rabia, I do not know how I would have kept my sanity these past four years without you. I also must thank my family. To Mom, Dad, and Seuss, I doubt I would ever have made it this far without you guys. Thank you for always being there for me, for pushing me to do my best, and for helping me through all the rough times.

Contents

1 Introduction.....	12
1.1 Motivation.....	12
1.2 The kinematic theory of fixed separation in unsteady flows.....	15
2 Methodology.....	17
2.1 The rotor-oscillator flow.....	17
2.2 Experimental apparatus.....	18
2.2.1 Physical apparatus.....	19
2.2.2 Fluid used for experiments.....	20
2.2.3 Flow visualization technique.....	21
2.3 Numerical techniques for flow simulation.....	23
2.4 Unsteady flow generation.....	24
2.4.1 Quasi-periodic flows.....	24
2.2.2 Aperiodic flows.....	26
3 Results.....	27
3.1 Experimental results.....	27
3.1.1 Fixed separation in unsteady, quasi-periodic flows.....	27
3.1.2 Fixed separation in unsteady, aperiodic flows.....	34
3.1.3 Comparison of separation in quasi-periodic and aperiodic flows.....	37
3.2 Numerical results.....	38
3.2.1 Comparison of numerical and experimental results.....	38
4 Conclusions.....	40
A Motor control logic.....	42
A.1 Motor control logic for quasi-periodic signals.....	42
A.2 Motor control logic for aperiodic signals.....	43
B Quasi-periodic flow generation.....	46
B.1 Generated quasi-periodic signals with incommensurate frequencies and phase shifts....	46
B.1.1 Quasi-periodic signal of RMS amplitude 0.38 mm.....	46
B.1.2 Quasi-periodic signal of RMS amplitude 0.81 mm.....	46

B.1.3 Quasi-periodic signal of RMS amplitude 1.54 mm.....	49
B.1.4 Quasi-periodic signal of RMS amplitude 2.36 mm.....	49
B.1.5 Quasi-periodic signal of RMS amplitude 2.99 mm.....	49
B.1.6 Quasi-periodic signal of RMS amplitude 3.83 mm.....	49
B.2 Generated quasi-periodic signals with equal frequencies and phase shifts	54
C Aperiodic flow generation.....	55
C.1 Generated random signals.....	55
C.1.1 Random signal of RMS amplitude 2 mm	55
C.1.2 Random signal of RMS amplitude 2.99 mm	55
C.1.3 Random signal of RMS amplitude 4 mm	57
C.1.4 Random signal of RMS amplitude 6 mm	57
C.1.5 Random signal of RMS amplitude 8 mm	59
C.1.6 Random signal of RMS amplitude 10 mm	59
References.....	62

List of Figures

1-1	Separation profile in an unstable flow that is viewed as an unstable manifold originating from a fixed point $\mathbf{p} = (\gamma, 0)$ on a boundary. Figure taken from Haller (2004).....	15
2-1	Cross-section of rotor-oscillator flow developed by Hackborn, Ulucakli, & Yuster (1997) to study flow mixing and separation in Stokes flows. Figure taken from Hackborn, Ulucakli, & Yuster (1997).....	17
2-2	The experimental apparatus utilized in this study.....	19
2-3	Optical setup used to produce 490 nm wavelength light column. M01, M02, M03 were all 1 inch diameter Vis Dielectric Model 5101 mirrors from New Focus, and L01 was a collimating lens rated at AR.14-50 mm.....	22
2-4	Plot of autocorrelation versus the number of time lags of the autocorrelation computed for (a) the function $f(t) = \sin(t)$ sampled at 100 Hz for 500 seconds, and (b) an arbitrary signal generated using a random number generator with maximum allowable amplitude 10 mm sampled at 100 Hz for 500 seconds.....	25
3-1	Separation profile produced by a quasi-periodic driving signal of RMS amplitude 0.81 mm.....	27
3-2	(a) Quasi-periodic signal of RMS amplitude 0.38 mm used to drive the translational motion of the cylinder, and (b) the autocorrelation of the same signal sampled at 1000 Hz for 343.67 seconds. The mean value and RMS amplitude are shown on the plot of the signal.....	28
3-3	Separation profile generated using the quasi-periodic signal with RMS amplitude 2.99 mm at (a) $t = 258.33$ seconds, (b) $t = 301.33$ seconds, and (c) $t = 322$ seconds. The angle of separation relative to the boundary is at the (a) median value, (b) largest value, and (c) smallest value. The separation point has been marked on each image.....	30
3-4	Fixed separation location in quasi-periodic flow with uncertainty in measurement. The ‘unique’ signals had incommensurate frequencies and phase shifts, and the ‘scaled’ signals had equal frequencies and phase shifts.....	31

3-5	Translational position of the cylinder driven by quasi-periodic signals of RMS amplitude (a) 2.36 mm and (b) 2.99mm. The mean value and RMS amplitude are shown on the plot of each signal.....	32
3-6	Skin friction profile along the boundary in a steady flow.....	33
3-7	(a) Random signal of RMS amplitude 10 mm used to drive the translational motion of the cylinder, and (b) the autocorrelation of the same signal sampled at 25 Hz for 350 seconds. The mean value and RMS amplitude are shown on the plot of the signal.....	35
3-8	Separation profile generated using the random signal with RMS amplitude 8 mm at (a) $t = 255.33$ seconds, (b) $t = 319.33$ seconds, and (c) $t = 343.67$ seconds. The angle of separation relative to the boundary is at the (a) smallest value, (b) median value, and (c) largest value. The separation point has been marked on each image.....	36
3-9	Comparison of measured separation location for the quasi-periodic and aperiodic flows investigated.....	37
3-10	Comparison of the separation location results obtained using dye visualizations and using numerical simulation of the Haller (2004) criteria.....	39
A-1	LabView wiring diagram used with quasi-periodic signals to control the motor that translates the cylinder. The true-false structures are set to false.....	42
A-2	LabView wiring diagram used with quasi-periodic signals to control the motor that translates the cylinder. The true-false structures are set to true.....	43
A-3	LabView wiring diagram used when generating aperiodic signals to control the motor that translates the cylinder. The true-false structures are set to false.....	44
A-4	LabView wiring diagram used when generating aperiodic signals to control the motor that translates the cylinder. The true-false structures are set to true.....	45
B-1	(a) Quasi-periodic signal of RMS amplitude 0.38 mm used to drive the translational motion of the cylinder, and (b) the autocorrelation of the same signal sampled at 1000 Hz for 343.67 seconds. The mean value and RMS amplitude are shown on the plot of the signal.....	47
B-2	(a) Quasi-periodic signal of RMS amplitude 0.81 mm used to drive the translational motion of the cylinder, and (b) the autocorrelation of the same signal sampled at 1000 Hz for 343.67 seconds. The mean value and RMS amplitude are shown on the plot of the signal.....	48

B-3	(a) Quasi-periodic signal of RMS amplitude 1.54 mm used to drive the translational motion of the cylinder, and (b) the autocorrelation of the same signal sampled at 1000 Hz for 343.67 seconds. The mean value and RMS amplitude are shown on the plot of the signal.....	50
B-4	(a) Quasi-periodic signal of RMS amplitude 2.36 mm used to drive the translational motion of the cylinder, and (b) the autocorrelation of the same signal sampled at 1000 Hz for 343.67 seconds. The mean value and RMS amplitude are shown on the plot of the signal.....	51
B-5	(a) Quasi-periodic signal of RMS amplitude 2.99 mm used to drive the translational motion of the cylinder, and (b) the autocorrelation of the same signal sampled at 1000 Hz for 343.67 seconds. The mean value and RMS amplitude are shown on the plot of the signal.....	52
B-6	(a) Quasi-periodic signal of RMS amplitude 3.83 mm used to drive the translational motion of the cylinder, and (b) the autocorrelation of the same signal sampled at 1000 Hz for 343.67 seconds. The mean value and RMS amplitude are shown on the plot of the signal.....	53
C-1	(a) Random signal of RMS amplitude 2 mm used to drive the translational motion of the cylinder, and (b) the autocorrelation of the same signal sampled at 25 Hz for 350 seconds. The mean value and RMS amplitude are shown on the plot of the signal.....	56
C-2	(a) Random signal of RMS amplitude 2.99 mm used to drive the translational motion of the cylinder, and (b) the autocorrelation of the same signal sampled at 25 Hz for 350 seconds. The mean value and RMS amplitude are shown on the plot of the signal.....	56
C-3	(a) Random signal of RMS amplitude 4 mm used to drive the translational motion of the cylinder, and (b) the autocorrelation of the same signal sampled at 25 Hz for 350 seconds. The mean value and RMS amplitude are shown on the plot of the signal.....	57
C-4	(a) Random signal of RMS amplitude 4 mm used to drive the translational motion of the cylinder to verify the results of the separation experiment conducted using the signal shown in Figure C-3, and (b) the autocorrelation of the same signal sampled at 25 Hz for 350 seconds. The mean value and RMS amplitude are shown on the plot of the signal.....	58

C-5	(a) Random signal of RMS amplitude 6 mm used to drive the translational motion of the cylinder, and (b) the autocorrelation of the same signal sampled at 25 Hz for 350 seconds. The mean value and RMS amplitude are shown on the plot of the signal.....	58
C-6	(a) Random signal of RMS amplitude 6 mm used to drive the translational motion of the cylinder to verify the results of the separation experiment conducted using the signal shown in Figure C-5, and (b) the autocorrelation of the same signal sampled at 25 Hz for 350 seconds. The mean value and RMS amplitude are shown on the plot of the signal.....	59
C-7	(a) Random signal of RMS amplitude 8 mm used to drive the translational motion of the cylinder, and (b) the autocorrelation of the same signal sampled at 25 Hz for 350 seconds. The mean value and RMS amplitude are shown on the plot of the signal.....	60
C-8	(a) Random signal of RMS amplitude 8 mm used to drive the translational motion of the cylinder to verify the results of the separation experiment conducted using the signal shown in Figure C-7, and (b) the autocorrelation of the same signal sampled at 25 Hz for 350 seconds. The mean value and RMS amplitude are shown on the plot of the signal.....	60
C-9	(a) Random signal of RMS amplitude 10 mm used to drive the translational motion of the cylinder, and (b) the autocorrelation of the same signal sampled at 25 Hz for 350 seconds. The mean value and RMS amplitude are shown on the plot of the signal.....	61

List of Tables

3.1	RMS amplitude and peak values of the set of six quasi-periodic signals with incommensurate frequencies and phase shifts used to drive the translational motion of the cylinder. The peak values given are the most negative and most positive positions in the signal.....	28
3.2	RMS amplitude and peak values of the set of six quasi-periodic signals with equal frequencies and phase shifts used to drive the translational motion of the cylinder. The peak values given are the most negative and most positive positions in the signal.....	29
3.3	RMS amplitude and peak values of the set of six random signals generated to drive the translational motion of the cylinder. The peak values given are the most negative and most positive positions in the signal.....	35
B.1	Frequency and phase shift for each sinusoidal component of the quasi-periodic signal of RMS amplitude 0.38 mm used to drive the translational motion of the cylinder for separation experiments.....	47
B.2	Frequency and phase shift for each sinusoidal component of the quasi-periodic signal of RMS amplitude 0.81 mm used to drive the translational motion of the cylinder for separation experiments.....	48
B.3	Frequency and phase shift for each sinusoidal component of the quasi-periodic signal of RMS amplitude 1.54 mm used to drive the translational motion of the cylinder for separation experiments.....	50
B.4	Frequency and phase shift for each sinusoidal component of the quasi-periodic signal of RMS amplitude 2.36 mm used to drive the translational motion of the cylinder for separation experiments.....	51
B.5	Frequency and phase shift for each sinusoidal component of the quasi-periodic signal of RMS amplitude 2.99 mm used to drive the translational motion of the cylinder for separation experiments.....	52

B.6	Frequency and phase shift for each sinusoidal component of the quasi-periodic signal of RMS amplitude 3.83 mm used to drive the translational motion of the cylinder for separation experiments.....	53
B.7	Required amplitude for each sinusoidal component of the signal described in Appendix B.1.5 necessary to produce specified RMS amplitude of signal.....	54

Chapter 1

Introduction

1.1 Motivation

Flow separation has a tremendous effect on the performance of aerospace and marine vehicles. Monitor and control of these flow separations is critical since aerospace and marine vehicles are performance limited by such separation. Thus, in order to forge ahead in the design of new, highly agile and extremely efficient machines, an exhaustive understanding of flow separation is required.

Presently, steady flow separation is a generally well understood concept. Prandtl (1904) showed that laminar boundary layer flow separation in a steady two-dimensional flow occurs at a point on the boundary where the skin friction vanishes and admits a negative gradient. Thus, if we define the x -direction tangent to the boundary and the y -direction normal to the boundary, then separation occurs at a point $\mathbf{p}(x,y) = (y,0)$ if:

$$\left. \begin{array}{l} \tau_w(\gamma) = 0, \\ \tau_{w,x}(\gamma) < 0, \end{array} \right\} \quad (1.1)$$

where τ_w is the skin friction along the boundary and $\tau_{w,x}$ is the skin friction gradient with respect to the x -direction. Furthermore, Lighthill (1963) found that the angle of separation, α , is given by:

$$\tan(\alpha) = \frac{-3\tau_{w,x}(\gamma)}{p_x(\gamma,0)}, \quad (1.2)$$

where p_x is the pressure gradient with respect to the x -direction.

The Prandtl (1904) and Lighthill (1963) criteria are not limited to boundary-layer separation, though. Rather, they can be applied to determine separation in any laminar, two-dimensional, steady flow including a separation bubble within a boundary layer (Young & Horton 1966), as well as separating streamlines in Stokes flow such as Moffatt corner-eddies (Moffatt 1964) or the rotor-oscillator flow (Hackborn, Ulucakli, & Yuster 1997).

Rott (1956), Moore (1958), Sears & Telionis (1971), and Haller (2004) have all shown through numerical simulations of boundary layer separation that while the Prandtl (1904) and Lighthill (1963) criteria provide a good understanding of steady, laminar, two-dimensional flow separation, both are unreliable indicators when dealing with unsteady flows. In fact, a generally accepted, proven set of criteria for identifying unsteady flow separation does not exist. Nor does a generally accepted definition for ‘separation’ exist in the unsteady case. For the purposes of the study presented here, though, the definition put forth by Prandtl is used, and ‘separation’ simply means the existence of a sharp, material spike of characteristic width, δ , and height, $h \gg \delta$, where fluid is suddenly ejected near a rigid boundary.

When observing that the Prandtl (1904) criterion did not correctly predict separation in unsteady flows, Sears & Telionis (1975) proposed an alternative separation criterion now known as the Moor-Rott-Sears (MRS) principle. The MRS principle states that unsteady separation occurs at a point off of the boundary where instantaneously the skin friction vanishes and the local velocity equals the velocity of the separation structure. But, this criterion is impractical to apply since a priori knowledge of the velocity of the separation structure is required as well as knowledge of variables away from the boundary (Williams 1977 and Van Dommelen 1981). Also, the MRS principle places separation points off of the boundaries, which is entirely useless from a control view as separation control is sensed and actuated off of the boundary (Wu et al.

2000). Furthermore, for truly unsteady flows, the time integrated effect of the unsteady streamlines on the fluid flow must be considered to determine material transport away from the boundary.

Van Dommelen (1981) and Van Dommelen & Shen (1982) proposed a Lagrangian approach to unsteady flow separation. Their work found that unsteady flow separation occurs at a point where a singularity occurs in the boundary layer equations. While Van Dommelen (1981) and Van Dommelen & Shen (1982) were able to remove difficulties found in the Eulerian approach while also proving the Lagrangian nature of unsteady flow separation, Liu & Wan (1985) found analytically that no direct correlation exists between separation in the boundary layer equations and velocity singularities.

Continuing the use of the Lagrangian approach, Shariff, Pilliam, & Ottino (1991) proposed a new theory to describe flow separation in two-dimensional, incompressible, time-periodic flows. By defining the separation point as a fixed point on the boundary with an unstable manifold in the Poincaré map of the periodic flow, the authors showed that unsteady flow separation occurs at points on the boundary where the time-averaged skin friction vanishes. Yuster & Hackborn (1997) re-derived the zero-mean-friction principle in a more mathematically rigorous way for near-steady, time-periodic, incompressible flows, and Hackborn, Ulucakli, & Yuster (1997) proved the result experimentally. Based on this body of work, Haller (2004) proposed a kinematic theory of unsteady separation for two-dimensional, compressible flows with arbitrary time dependence. It is the goal of this study to investigate the Haller (2004) criterion for fixed separation in quasi-periodic, two-dimensional flows.

1.2 The kinematic theory of fixed separation in unsteady flows

In his kinematic theory of fixed separation in unsteady flows, Haller (2004) implements a dynamical systems approach to fixed separation in an unsteady, two-dimensional flow. As shown in Figure 1-1, the separation profile, $M(t)$, in this approach is an unstable manifold that originates from a fixed separation point, γ , located on the boundary. Qualitatively, the separation profile is simply a distinguished material line that attracts fluid particles and ejects them away from the boundary.

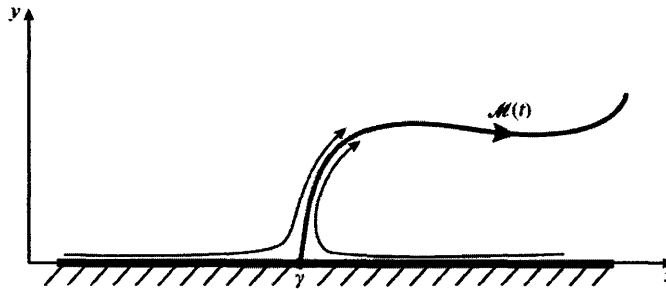


Figure 1-1: Separation profile in an unstable flow that is viewed as an unstable manifold originating from a fixed point $\mathbf{p} = (\gamma, 0)$ on a boundary. Figure taken from Haller (2004).

Haller (2004) states that in an incompressible flow, a fixed separation point occurs on a no-slip boundary at the location where the time averaged skin friction vanishes and the time averaged skin friction gradient is negative. Thus, any fixed separation point $\mathbf{p}(x, y) = (\gamma, 0)$ satisfies the following criteria at time t_0 :

$$\left. \begin{aligned} \int_{-\infty}^{t_0} \tau_w(\gamma, t) dt &= 0, \\ \int_{-\infty}^{t_0} \tau_{w,x}(\gamma, t) dt &< 0. \end{aligned} \right\} \quad (1.3)$$

The criterion (1.3) can be generalized to any mass-conserving fluid flow.

The first condition presented in (1.3) is a necessary condition for a material separation or re-attachment profile to exist at point \mathbf{p} . The second condition presented in (1.3) serves to ensure material ejection from point \mathbf{p} into the fluid flow, thus differentiating point \mathbf{p} from a re-attachment point. The second condition is also related to the strength of the separation, and thus can be used to differentiate between small-scale separation and boundary layer separation in a physical situation. Furthermore, for steady, incompressible flows, the Haller criterion (1.3) simplifies to the Prandtl criterion (1.1).

Haller (2004) also proposed an analytic formula to determine the time-dependent orientation of the separation profile, or the angle of separation, α . At any time t_0 , the angle of separation, α , can be calculated from distributed skin friction and pressure measurements by:

$$\tan(\alpha) = \frac{3 \int_{t_0}^{-\infty} \tau_{w,x}(\gamma, t) dt}{\int_{t_0}^{-\infty} \left[p_x(\gamma, 0, t) + 3\tau_{w,x}(\gamma, t) \int_{t_0}^t \frac{1}{\nu\rho} \tau_w(\gamma, t) ds \right] dt}, \quad (1.4)$$

where ν is the kinematic viscosity of the fluid and ρ is the density of the fluid. In the limit of steady flow, the Haller criterion (1.4) simplifies to the Lighthill criterion (1.2). Similarly to criterion (1.3), criterion (1.4) can be generalized to any mass-conserving fluid flow.

Chapter 2

Methodology

2.1 The rotor-oscillator flow

The experimental arrangement we utilized in this study was the rotor-oscillator flow that Hackborn, Ulucakli, & Yuster (1997) developed to study flow mixing and separation in Stokes flows. The experimental apparatus used by Hackborn, Ulucakli, & Yuster (1997) consisted of a rotating cylinder immersed in a tank. Oscillating the sidewall of the tank introduced unsteadiness, and the resultant flow was two-dimensional. Figure 2-1 displays a cross-section of the flow generated by this apparatus:



Figure 2-1: Cross-section of rotor-oscillator flow developed by Hackborn, Ulucakli, & Yuster (1997) to study flow mixing and separation in Stokes flows. Figure taken from Hackborn, Ulucakli, & Yuster (1997).

Hackborn, Ulucakli, & Yuster (1997) demonstrated that unsteady flow separation in the rotor-oscillator flow occurs on time scales on the order of seconds and length scales on the order of centimeters, which both facilitate visualization and simulation of the separation. Also, Hackborn, Ulucakli, & Yuster (1997) showed that the rotational speed of the cylinder and the oscillation of the sidewall both control the resultant flow separation, which are both favorable to

the experimental investigation as they allow for relatively easy manipulation of the separation. Ultimately, the rotor-oscillator flow represents the simplest method to study unsteady flow separation as other experimental arrangements tend to be impractically large and inefficient in these types of studies.

To generate the rotor-oscillator flow in this study, we used a cylinder immersed into a tank and capable of rotational motion about its axis and translational motion parallel to the front wall of the tank. This differs from the apparatus Hackborn, Ulucakli, & Yuster (1997) utilized since unsteadiness in the flow is introduced by translating the rotating cylinder as opposed to the front wall of the tank, which remains stationary in our arrangement. This difference was intentional as it allowed more flexibility and control over the unsteadiness introduced into the flow. In spite of this difference, the rotor-oscillator flow generated remains similar to that utilized by Hackborn, Ulucakli, & Yuster (1997) since the flow is still expected to be nominally two-dimensional, and flow separation occurs at the front wall of the tank. In this arrangement, the location of separation is controlled by the characteristics of the rotational and translational motion of the cylinder.

2.2 Experimental apparatus

A diagram of the experimental apparatus is shown in Figure 2-2:

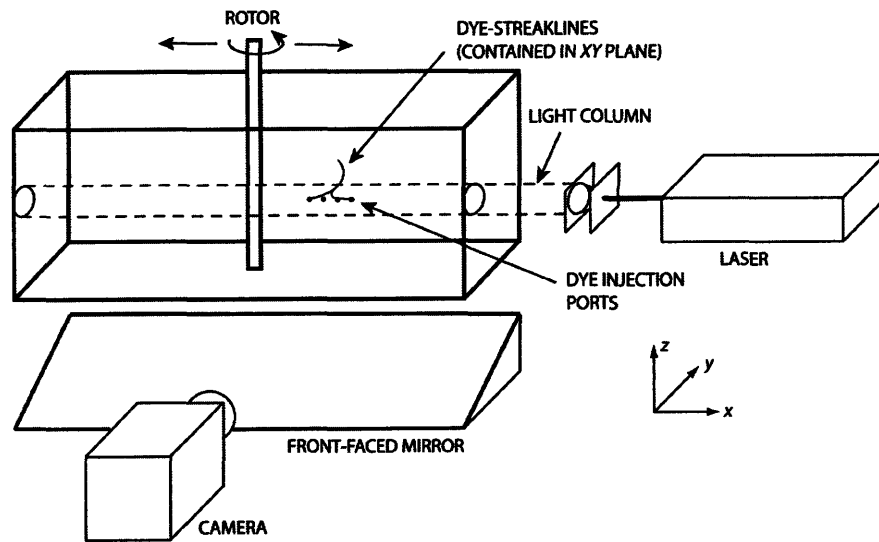


Figure 2-2: The experimental apparatus utilized in this study.

2.2.1 Physical apparatus

The experimental apparatus comprised an acrylic tank that sat within an aluminum support frame with leveling mounts that elevated the tank approximately 20 cm from ground level. The tank was leveled using a Starett level model #98. The acrylic tank itself had dimensions 40.2 cm long, 10.0 cm wide, and 12.0 cm deep. The top of the tank remained open to create a free surface on top of the fluid, and a 1.2 cm thick acrylic sheet that contained a dye injection port system for flow visualizations (described in detail in Section 2.2.3) was placed along the front wall of the tank. The addition of the dye injection wall gave the tank a nominal width of 8.8 cm and left the other dimensions unaltered.

The rotor-oscillator flow was driven using a cylinder of diameter 6.39 mm that was positioned vertically in the tank such that 26.20 ± 0.25 mm were between the center of the cylinder and the dye injection wall aligned flush to the 40.2 cm front wall. For each experimental run, we also initially placed the cylinder at a location between the 10.0 cm side walls defined by the flow visualization technique (see Section 2.2.3). The cylinder extended

down into the tank to within 1.0 cm of the bottom wall, and was aligned to be true to within 0.13 mm relative to the axis of rotation of the cylinder by using a Starrett dial test indicator with stylus accurate to 0.001 inches. The top of the cylinder was attached to a stepper motor that drove the rotational motion, and the stepper motor was attached to a horizontal translation stage that was aligned parallel to the front wall to within ± 0.25 mm at either end. For all experimental runs, the cylinder's rate of rotation was maintained at 20.89 rad/s (199.5 RPM). The horizontal trajectory of the cylinder was determined by a generated quasi-periodic signal (see Section 2.4).

The stepper motor used to provide rotational motion to the cylinder was an Intelligent Motion Systems (IMS) IOS34 inside-out stepper motor monitored by an IMS optical encoder with a single end encoder connection. An IMS IM805 micro-stepping driver drove the inside-out stepper motor. The horizontal translation stage was a LINTECH linear stage 10 inches in length that comprised a 0.25 inch diameter lead screw rotated by an IMS MDrive23 stepper motor with a built in micro-stepper driver and encoder. Both stepper motors were powered by IMS IP804 power supplies and controlled using the commercial software package LabVIEW 7 via a National Instruments PCI-7344 motion card. Details of the specific control logic utilized can be found in the Appendix.

2.2.2 Fluid used for experiments

We selected glycerol as our fluid of interest because we needed a viscous fluid to maintain a low Reynolds number to ensure that the time scales of our experiments would be long enough to be conducive to visualization. The glycerol had a density of 1262 kg/m^3 and a kinematic viscosity of $9 \times 10^{-4} \text{ m}^2/\text{s}$. The kinematic viscosity was measured using an Anton Parr DMA 38 rheometer at a temperature of 20°C .

Early observations suggested that the interaction between the cylinder and tank bottom produced pronounced three-dimensional effects in the visualization region. To combat these effects, a layer of FC-40 Fluorinert electronic coolant produced by 3M was added below the glycerol. FC-40 was selected because of its immiscibility to glycerol as well as its high density (1900 kg/m^3) and low viscosity ($2 \times 10^{-6} \text{ m}^2/\text{s}$) relative to glycerol. In addition to the FC-40 layer, a thin layer of vegetable oil was added on top of the glycerol in order to prevent the hydrophilic glycerol from absorbing moisture from air thereby decreasing its viscosity.

With the dye injection wall in place in the tank, the thickness of the glycerol layer was set to 5.0 cm because experimental and theoretical results suggested that a 5.0 cm layer was large enough to suppress surface effects and maintain nominal two-dimensional flow in the visualization region. The FC-40 layer was then set at 2.8 cm in order to center the glycerol layer at the dye injection ports (see Section 2.2.3 for more details regarding the flow visualization technique).

2.2.3 Flow visualization technique

Flow visualization occurred by observing the streaklines created by a neutrally buoyant, fluorescent dye. The dye used was a mixture of glycerol and fluorescein. The concentration of fluorescein was kept as minimal as possible so as to not noticeably affect the density of the glycerol. Fluorescein was selected because the minimal concentration required to not noticeably affect the density and neutral buoyancy of the dye was still acceptable to achieve the level of fluorescence necessary for imaging. The dyed fluid maintained two-dimensional flow over the entire period of an experimental run (343.67 seconds) since no vertical motion was detectable.

The dye was mechanically injected into the mid-depth of the tank via a port system contained in the 1.2 cm thick acrylic sheet placed flush to the 40.2 cm tank wall. The port

system comprised four injection ports of exit diameter 0.56 mm placed approximately 13.3 mm apart at the mid-depth of the tank. Dye was supplied at a rate of 1 mL/hour to the port system by a 25 mm diameter syringe controlled using a Cole-Parmer Instrument Company 74900 series injection pump. In order to not affect the flow near the region of separation, the cylinder was initially placed between the 10.0 cm side walls of the tank such that the separation location was located at least several millimeters away from any injection port.

The fluorescein in the dye was excited using a light column of wavelength 490 nm produced by a Coherent Infinity laser that pulsed 450 mJ IR energy light at 20 Hz. The light column was placed to illuminate fluid near the front wall of the tank so that the separation region could be easily observed. Figure 2-3 displays the optical setup utilized to produce the 490 nm wavelength light column:

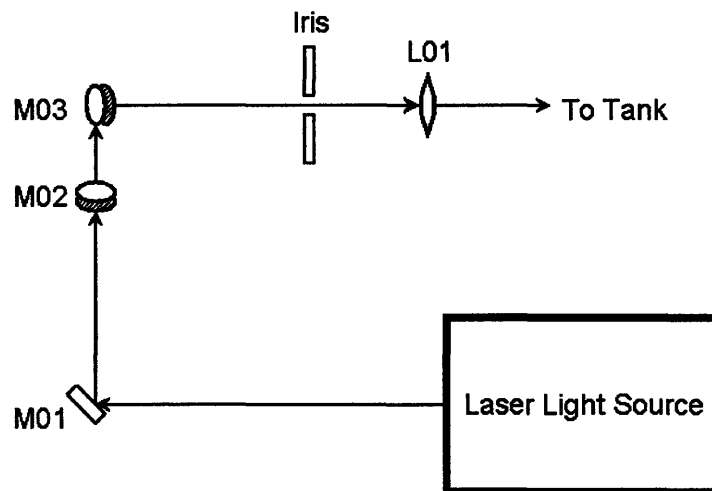


Figure 2-3: Optical setup used to produce 490 nm wavelength light column. M01, M02, M03 were all 1 inch diameter Vis Dielectric Model 5101 mirrors from New Focus, and L01 was a collimating lens rated at AR.14-50 mm.

A LaVision Imager ProX CCD camera that viewed the flow through a 45° front-faced mirror beneath the tank captured the evolution of the dyed fluid flow. The CCD camera was fitted with a Nikon AF Micro Nikkor 105 mm, 1:2.8 D lens and a 532 nm bandpass filter that

allowed the camera to record only the 530 nm wavelength light emitted from the excited dye molecules. The images recorded by the CCD camera were recorded directly to a computer with a LaVis software package version 7 that was used to process the recorded data. Image acquisition was triggered by the rotor-oscillator flow motion control 240 seconds after the cylinder began its horizontal translation so that each image time step could be matched to the numerical simulation. To account for parallax, calibration occurred by imaging a ruler in the horizontal mid-depth plane of the tank. This process resulted in a calibration factor that related millimeters to image pixels and allowed accurate scaling in millimeters.

2.3 Numerical techniques for flow simulation

The numerical simulations were completed using an incompressible solver with dynamic mesh provided by the Fluent software package version 6.1. When computing the flow field, the cylinder was used as a reference point, which required that the tank wall as opposed to the cylinder oscillated. While using the cylinder as a reference point creates a numerical scenario that differs from the experimental conditions, the alternatives are computationally less efficient and accurate. A fixed boundary-fitted mesh was then used around the cylinder, and an orthogonal, dynamic mesh was used near the tank wall. The orthogonal, dynamic mesh allowed for relatively simple and accurate implementation in the numerical simulations. We note that in the cylinder reference frame, a time dependent source appears in the Navier-Stokes equations (Fumagalli 2002).

After the flow field was computed, skin-friction and pressure gradient profiles were extracted from the numerical simulations. Using these quantities, the location of separation and angle of separation in the flow were calculated using the criterion specified in (1.1) – (1.4). These predictions could then be compared with the experimental and theoretical results.

2.4 Unsteady flow generation

2.4.1 Quasi-periodic flows

Numerical techniques used for flow simulations are limited by the fact that computing a flow field requires precisely defined equations. Thus, to gain insight into aperiodic flow separation, we must be able to mimic a truly random flow without the use of a random number generator when defining the translational motion of the cylinder. An appropriate method to mimic a random signal is to use a summation of sinusoids each of unique frequency and phase shift. Therefore, signals of the following form were used to define the motion of the cylinder:

$$y(t) = \sum_{i=0}^N a_i \sin(\omega_i t + \phi_i), \quad (2.1)$$

where y is the position of the cylinder on the axis parallel to the 40.2 cm wall of the tank, t is time, a is the amplitude of each sinusoidal component of the signal, ω is the frequency of each sinusoidal component of the signal, ϕ is the phase shift of each sinusoidal component of the signal, and N is the number of sinusoidal components that make up the signal.

To measure the random quality of the generated signal, the autocorrelation function was implemented. The autocorrelation function determines the periodicity of a function by comparing the function with a time shifted version of itself. The autocorrelation function of the position of the cylinder, y , is defined by:

$$R_f(t) = \lim_{T \rightarrow \infty} \left(\frac{1}{2T} \int_{-T}^T y(\tau) y(t + \tau) d\tau \right), \quad (2.2)$$

where $R_f(t)$ is the autocorrelation of the function $y(t)$, T is an arbitrary time variable, and τ and is the desired time lag. Figure 2-4 offers a comparison between a plot of the autocorrelation versus

the number of time lags of the autocorrelation computed for the periodic signal $\sin(t)$ and the same plot computed for a truly random signal with maximum amplitude 10 mm:

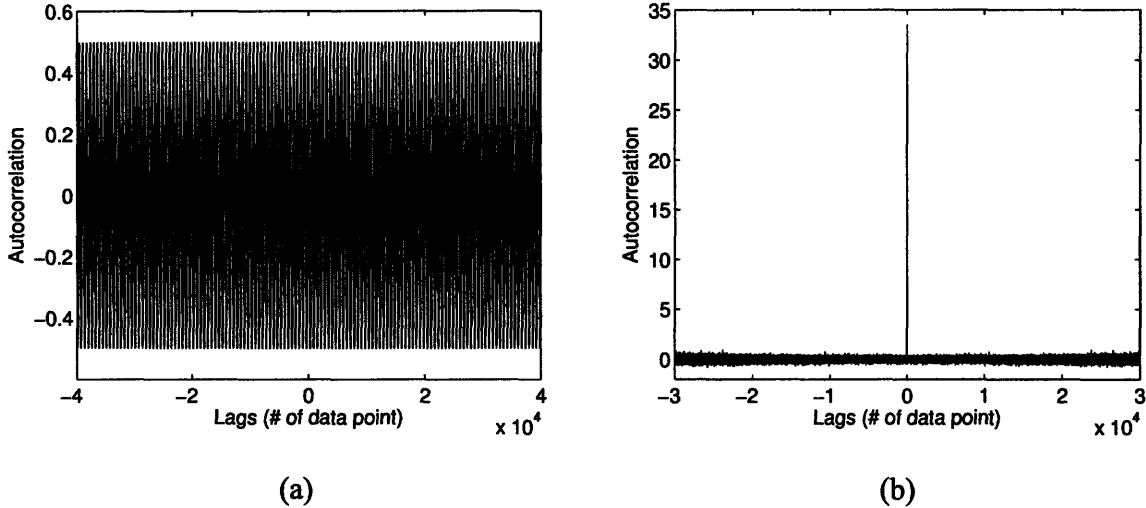


Figure 2-4: Plot of autocorrelation versus the number of time lags of the autocorrelation computed for (a) the function $f(t) = \sin(t)$ sampled at 100 Hz for 500 seconds, and (b) an arbitrary signal generated using a random number generator with maximum allowable amplitude 10 mm sampled at 100 Hz for 500 seconds.

As Figure 2-4 displays, the random quality of a signal can be determined directly by the drop off of the plot of the autocorrelation versus number of time lags of the autocorrelation computed for a signal of interest. Based on early observations, signals with $N > 20$ sinusoids did not produce a sizable enough drop in the autocorrelation to justify the added computational workload. Therefore, signals with $N = 20$ sinusoids were generated to define the cylinder's motion.

When generating the desired signals for this study, the amplitude of each sinusoidal component was kept constant to ensure control over the RMS amplitude of the resulting signal. A random number generator was used to select the frequency and phase shift for each sinusoidal component in order to ensure a sharper drop off in the autocorrelation of the signal. The allowable range of frequency selections was defined by the amplitude of the desired signal since

larger amplitudes required lower frequencies so that the motor would be able to accommodate the accelerations generated. The allowable range of phase shifts was set to between $-\pi/2$ and $\pi/2$. Details of each signal generated can be found in the Appendix.

2.2.2 Aperiodic flows

Even though we were unable to simulate aperiodic flows using numerical techniques, we still wanted to investigate flow separation in this regime and compare it to flow separation in quasi-periodic flows. To produce an aperiodic flow, the cylinder was driven by a random signal waveform generated by the LabView software package version 7.0. The random signal waveform was created by sampling 8750 points of uniform white noise at 1000 Hz. The sampled signal was processed through a low-pass filter with a cutoff frequency selected so that the stepper motor that provided the cylinder's translational motion could accommodate the required accelerations. The processed signal was then scaled to a known RMS amplitude before the stepper motor read the signal at 25 Hz to produce an experimental run of 350 seconds. While all experimental runs in this study were 343.67 seconds in length, the additional 6.33 seconds were required because of the logic required to program a stepper motor. Details of each signal generated can be found in the Appendix.

Chapter 3

Results

3.1 Experimental results

A typical separation profile produced by the experimental apparatus and method used in this study is shown in Figure 3-1:

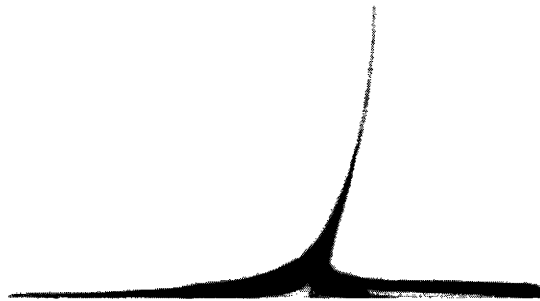


Figure 3-1: Separation profile produced by a quasi-periodic driving signal of RMS amplitude 0.81 mm.

As Figure 3-1 displays, the separation profile forms a dyed region near the boundary. Within this material region is an area of finite width devoid of dye. Based on the definition used to describe ‘separation,’ it was understood that the location of separation was contained within this empty region. The size of the empty region caused uncertainty that was viewed as the error bounds of the measurement of the separation location in this study.

3.1.1 Fixed separation in unsteady, quasi-periodic flows

The Haller criterion (1.3) states that fixed separation occurs in unsteady, quasi-periodic flows that can maintain a unique time averaged zero skin friction point as time progresses. To study fixed separation in unsteady, quasi-periodic flows, two sets of quasi-periodic signals were generated to drive the translational motion of the cylinder (see Section 2.4.1). The first set was

comprised of six signals with incommensurate frequencies and phase shifts. These signals were quantified using the root-mean-square (RMS) of their amplitudes over the duration of an experimental run which was approximately 343.667 seconds. Table 3.1 gives the RMS amplitude and peak values of each signal employed. Figure 3-2 displays the signal with RMS amplitude 0.38 mm and the autocorrelation of the same signal as a measure of its aperiodic quality. Details of each of the quasi-periodic signals employed can be found in the Appendix.

RMS Amplitude (mm)	Peak Value	
	Negative Position (mm)	Positive Position (mm)
0.38	-1.16	1.39
0.81	-2.39	2.86
1.54	-4.85	4.66
2.36	-7.54	7.23
2.99	-9.07	11.39
3.83	-12.01	13.93

Table 3.1: RMS amplitude and peak values of the set of six quasi-periodic signals with incommensurate frequencies and phase shifts used to drive the translational motion of the cylinder. The peak values given are the most negative and most positive positions in the signal.

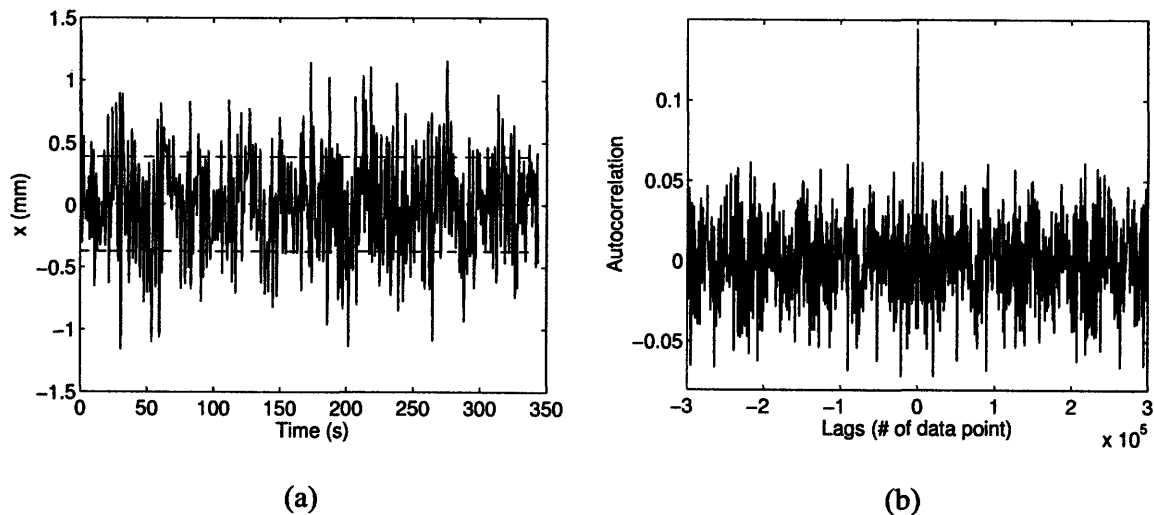


Figure 3-2: (a) Quasi-periodic signal of RMS amplitude 0.38 mm used to drive the translational motion of the cylinder, and (b) the autocorrelation of the same signal sampled at 1000 Hz for 343.67 seconds. The mean value and RMS amplitude are shown on the plot of the signal.

In addition to the set of six signals with differing frequencies and phase shifts, a second set of six quasi-periodic signals with equal frequencies and phase shifts were used to drive the translational motion of the cylinder. These signals were each scaled from the signal with RMS amplitude of 2.99 mm. This approach to signal generation was adopted in order to easily attain higher RMS amplitudes. Also, using signals with equal frequencies and phase shifts but differing amplitudes allowed for the effects of the signal geometry on separation location to be studied with more depth. Table 3.2 gives the RMS amplitude and peak values of each signal employed. Details of each of these signals can be found in the Appendix.

RMS Amplitude (mm)	Peak Value	
	Negative Position (mm)	Positive Position (mm)
2	-6.08	7.64
2.99	-9.07	11.39
4	-12.16	15.27
6	-18.24	22.91
8	-24.32	30.54
10	-30.40	38.18

Table 3.2: RMS amplitude and peak values of the set of six quasi-periodic signals with equal frequencies and phase shifts used to drive the translational motion of the cylinder. The peak values given are the most negative and most positive positions in the signal.

For both sets of signals, the cylinder was rotated at 199.5 RPM or 20.89 rad/s. Using the resulting tangential velocity of the cylinder, the diameter of the cylinder, and the kinematic viscosity of the glycerol, the Reynolds number of the generated flow was 0.47. With these parameters, a typical experimental run is shown below in Figure 3-3. The flow separation presented in Figure 3-3 was generated using the quasi-periodic signal with RMS amplitude of 2.99 mm to drive the translational motion of the cylinder. In the entire time series of images, the measured separation location is marked.

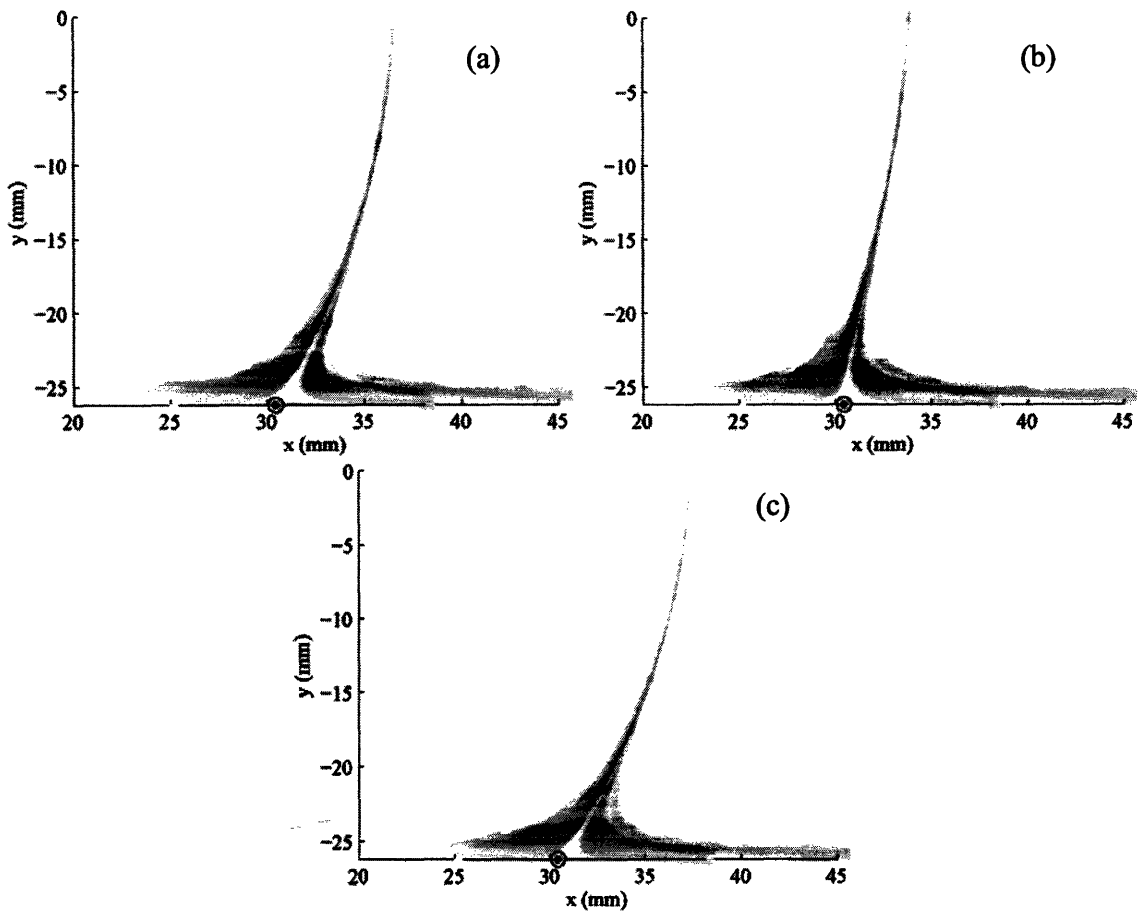


Figure 3-3: Separation profile generated using the quasi-periodic signal with RMS amplitude 2.99 mm at (a) $t = 258.33$ seconds, (b) $t = 301.33$ seconds, and (c) $t = 322$ seconds. The angle of separation relative to the boundary is at the (a) median value, (b) largest value, (c) smallest value. The separation point has been marked on each image.

As Figure 3-3 indicates, fixed separation is maintained throughout the duration of the experiment for the quasi-periodic signal with RMS amplitude of 2.99 mm. In fact, fixed separation was observed for each unsteady, quasi-periodic flow in this study. The location of fixed separation measured for each flow studied is displayed in Figure 3-4. Again, the error bars denote the size of the region devoid of dye within the dyed region near the wall. The apparent bias in the error bars is due to the asymmetrical shape of the region caused by the large jump in flow velocity that is expected across the separation spike.

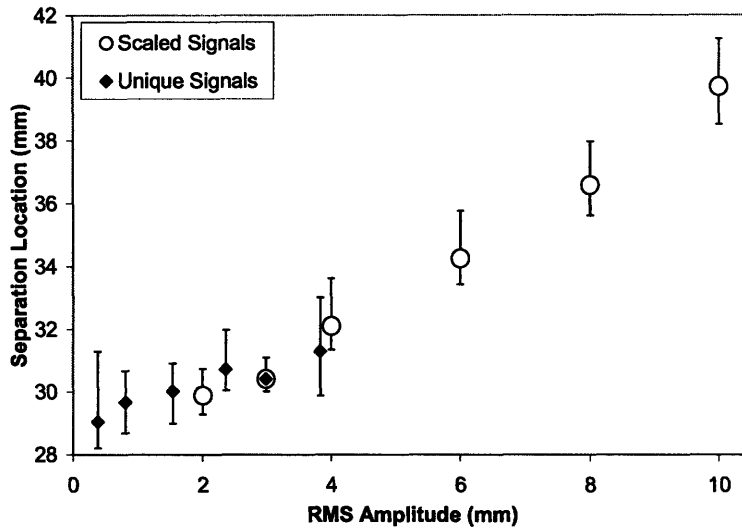


Figure 3-4: Fixed separation location in quasi-periodic flow with uncertainty in measurement. The ‘unique’ signals had incommensurate frequencies and phase shifts, and the ‘scaled’ signals had equal frequencies and phase shifts.

When we repeated any of the flows presented in Figure 3-4, we found that the measured fixed separation location always agreed to within 1%. Therefore, we are confident of the results shown. It is also important to note that the mean of the quasi-periodic signal used to drive the translational motion of the cylinder is not always the initial position of the cylinder at $t = 0$ of an experimental run from which the location of separation is measured. For the quasi-periodic cases presented, though, the mean is typically less than 0.1 mm, and so the separation location measurement should not be greatly affected.

As Figure 3-4 indicates, the location of separation relative to the initial cylinder location at $t = 0$ typically increases monotonically with the RMS amplitude of the translational motion of the cylinder. While this suggests that the amplitude of oscillation greatly affects the location of separation, the measured separation location twice decreases relative to the RMS amplitude despite the strength of the experimental results. Specifically, the measured separation location drops by approximately 0.1 mm between the flows driven by the signals with RMS amplitudes of

1.54 mm and 2 mm, and by approximately 0.3 mm between the flows driven by the signals with RMS amplitude of 2.36 mm and 2.99 mm. The relatively small difference between the separation locations for each respective pair suggests that separation occurs at essentially the same location for flows driven by both signals in the pair. Thus, the implication is that another factor of the translational motion plays a significant role in flow separation. Figure 3-5 compares the translational motion of the cylinder driven by the signals with RMS amplitudes of 2.36 mm and 2.99 mm:

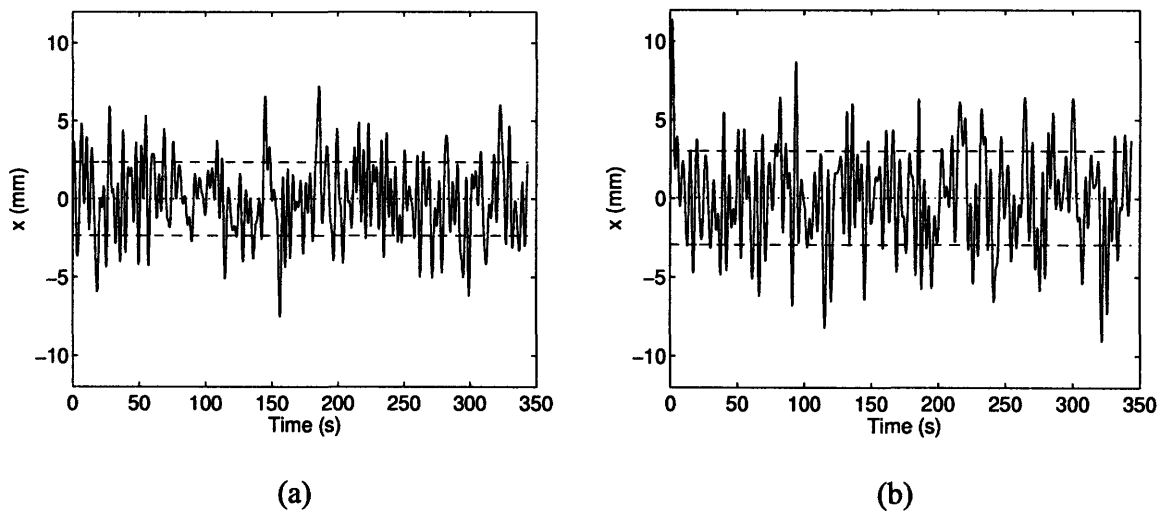


Figure 3-5: Translational position of the cylinder driven by quasi-periodic signals of RMS amplitude (a) 2.36 mm and (b) 2.99 mm. The mean value and RMS amplitude are shown on the plot of each signal.

Figure 3-5 shows that a cylinder driven by both signals typically remains within $x \sim \pm 3$ mm for the duration of an experimental run. However, while the cylinder rarely attains a position of $x = \pm 7$ mm when driven by the signal with RMS amplitude 2.36 mm, it exceeds the $x = \pm 7$ mm range four separate times when driven by the signal with RMS amplitude 2.99 mm. In fact, the furthest the cylinder travels when driven by the signal with RMS amplitude 2.99 mm is almost 12 mm from its initial position at $t = 0$. It is these peak values that effectively

differentiate the two signals in regards to the RMS amplitude. Because the peak values in the translational motion of the cylinder driven by the signal with RMS amplitude 2.99 mm occur on such a relatively fast time scale, the peak motions barely, if at all, affect the time averaged zero skin friction point of the flow. Therefore, the time averaged zero skin friction point of both flows should occur at roughly the same location. It then follows from the Haller criterion (1.3) that fixed separation should be located at the same location as well, which is precisely what occurs. This implies that the separation location is relatively immune to massive peak values in the translation motion of the cylinder. So, while using the RMS amplitude to describe each driving signal does not fully capture the physics of the resulting flow, we continue to use it since it is the best method available to compare results.

If we choose to disregard the ‘random’ nature of a quasi-periodic flow and its effect on the dynamics of the flow, we should expect to find that the location of separation does increase monotonically relative to the RMS amplitude of the signal driving the cylinder. This trend follows from the expected skin friction profile along the boundary. The skin friction profile along the boundary in a steady flow is shown in Figure 3-6:

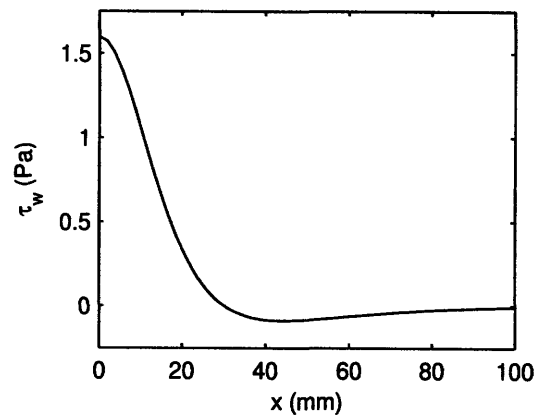


Figure 3-6: Skin friction profile along the boundary in a steady flow.

The skin friction profile is asymmetrical such that in absolute terms, the skin friction nearest the translating cylinder is higher than the corresponding skin friction farthest from the translating cylinder relative to the time averaged zero skin friction point. Thus, the net effect is that the translation of the cylinder ‘pushes’ the time averaged zero skin friction point further away from the cylinder’s initial position as the amplitude of oscillation increases. As Figure 3-4 shows, this is exactly what occurs with the flows driven by the scaled signals of equal frequencies and phase shifts. In fact, for the flows driven by the scaled signals, the separation location increases monotonically relative to RMS amplitude in an almost linear fashion. Ultimately, the original finding that a larger amplitude yields a separation point located farther from the initial position of the cylinder at $t = 0$ remains valid and further lends credence to the Haller criterion (1.3).

3.1.2 Fixed separation in unsteady, aperiodic flows

The Haller criterion (1.3) can also be extended to fixed separation in unsteady, aperiodic flows that maintain a unique time averaged zero skin friction point as time progresses. To study fixed separation in unsteady, aperiodic flows, the LabView software package version 7.0 was used to generate random signals at specified RMS amplitudes to drive the translational motion of the cylinder (see Section 2.4.2). Random signals with RMS amplitudes that corresponded to the six scaled quasi-periodic signals discussed in Section 3.1.1 were studied. Table 3.3 gives the RMS amplitude and peak values of each random signal that was generated. Figure 3-7 shows the random signal of RMS amplitude 10 mm that was used to drive the translational motion of the cylinder, as well as its autocorrelation. Details of all of the random signals generated can be found in the Appendix.

RMS Amplitude (mm)	Peak Value	
	Negative Position (mm)	Positive Position (mm)
2	-5.61	7.86
2.99	-8.41	8.27
4	-10.97	9.53
6	-12.39	19.13
8	-26.71	24.71
10	-24.57	33.84

Table 3.3: RMS amplitude and peak values of the set of six random signals generated to drive the translational motion of the cylinder. The peak values given are the most negative and most positive positions in the signal.

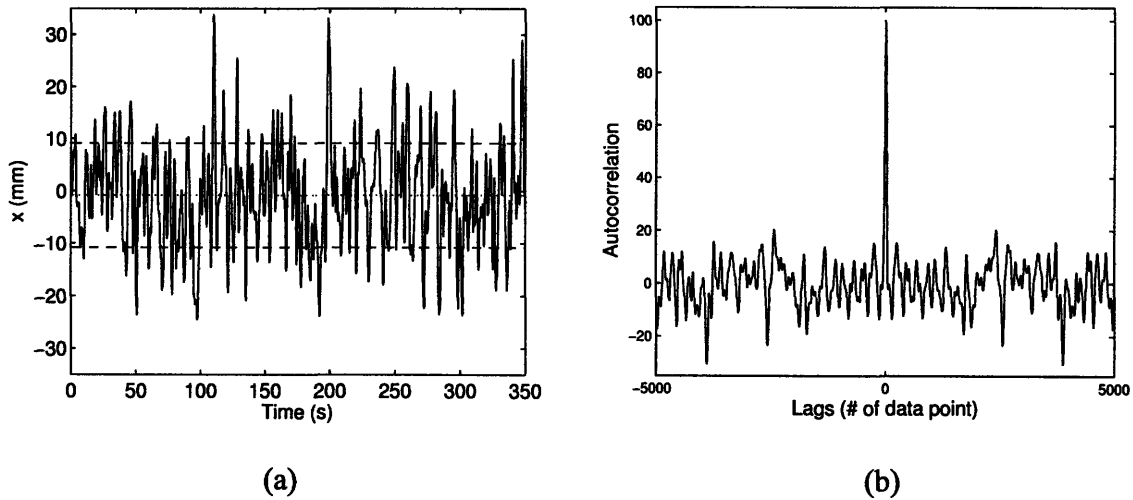


Figure 3-7: (a) Random signal of RMS amplitude 10 mm used to drive the translational motion of the cylinder, and (b) the autocorrelation of the same signal sampled at 25 Hz for 350 seconds. The mean value and RMS amplitude are shown on the plot of the signal.

As was previously done, the cylinder was rotated at 199.5 RPM or 20.89 rad/s, which resulted in a flow with a Reynolds number of 0.47. With these parameters, a typical experimental run is shown in Figure 3-8. The flow separation presented in Figure 3-8 was generated by driving the translational motion of the cylinder using the random signal of RMS amplitude 8 mm. Again, the measured separation location is marked.

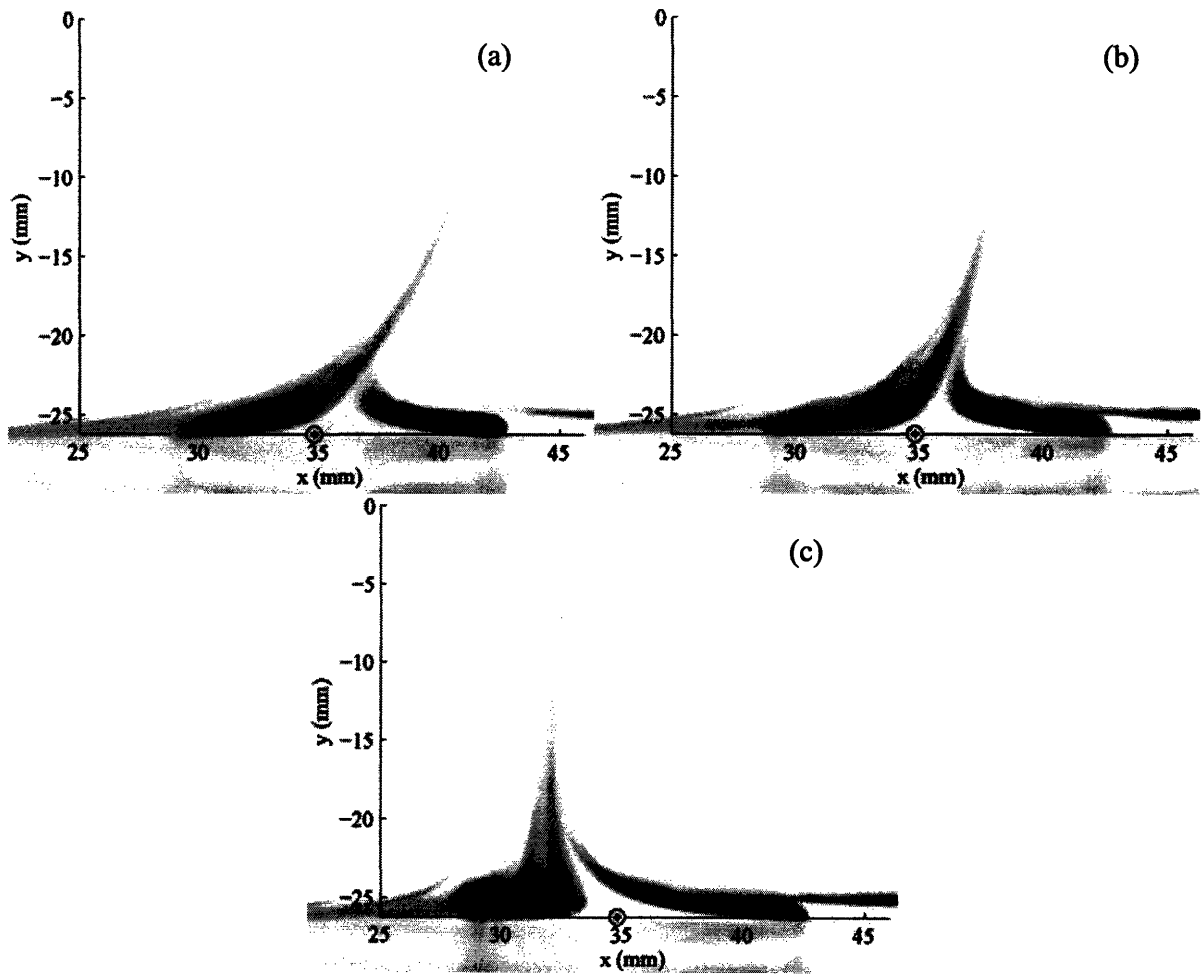


Figure 3-8: Separation profile generated using the random signal with RMS amplitude 8 mm at (a) $t = 255.33$ seconds, (b) $t = 319.33$ seconds, and (c) $t = 343.67$ seconds. The angle of separation relative to the boundary is at the (a) smallest value, (b) median value, and (c) largest value. The separation point has been marked on each image.

As Figure 3-8 indicates, fixed separation is maintained throughout the duration of the experiment for the random signal with RMS amplitude of 8 mm. Similarly to the quasi-periodic flows studied, each unsteady, aperiodic flow produced fixed separation. When we repeated these experiments using flows driven by different random signals of equal RMS amplitude, we measured separation locations that were $\sim 1\text{-}2\%$ different from the original result, thus proving the strength of our measurement.

3.1.3 Comparison of separation in quasi-periodic and aperiodic flows

Figure 3-9 offers a comparison between the measured separation location between corresponding quasi-periodic and aperiodic flows studied:

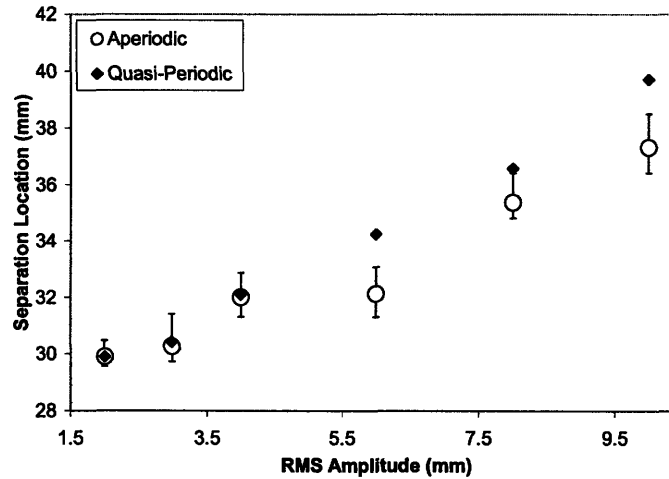


Figure 3-9: Comparison of measured separation location for the quasi-periodic and aperiodic flows investigated.

As Figure 3-9 shows, we again see a non-monotonic increase in the separation location relative to the RMS amplitude for the unsteady, aperiodic flows presented. Also, while the measured separation location for the quasi-periodic and aperiodic flows are in good agreement for smaller RMS amplitudes, a divergence occurs after the 4 mm RMS amplitude case. As discussed in Section 3.1.1, it is the ‘random’ nature of the signals used to drive the aperiodic flows that causes these discrepancies. The discrepancy becomes more pronounced for larger RMS amplitudes because generated random signals are more likely to incorporate massive peak position values in order to attain larger RMS amplitudes. Furthermore, unlike the signals used to drive the quasi-periodic flows, the signals used to drive the aperiodic flows do not necessarily have a mean value near the initial position of the cylinder at $t = 0$. In fact, the random signals used to drive the aperiodic flows have mean values up to 1.25 mm from the initial position of the

cylinder at $t = 0$. While this certainly affects a proper measurement of the separation location, it is difficult to determine the effect on the separation location due to nonlinearities in the skin friction profile.

Despite the difficulty in attaining a proper comparison of separation location between quasi-periodic and aperiodic flows using RMS amplitude, we can say that both types of flow exhibit the same general idea. Ultimately, larger amplitudes in the cylinder's translational motion cause separation to occur further from the initial position of the moving cylinder due to the 'pushing out' effect the motion has on the time averaged zero skin friction point, which further supports the Haller criterion (1.3) in a qualitative sense.

3.2 Numerical results

3.2.1 Comparison of numerical and experimental results

In order to study the Haller criterion (1.3) more quantitatively, numerical simulations were conducted and a theoretical separation location was measured from the result. Because a well defined function is required in order to simulate the flow field in a numerical simulation, a comparison could only be made with the measured separation location for the quasi-periodic flows studied. Figure 3-10 offers a comparison between the separation location found from the numerical simulations conducted and the corresponding quasi-periodic flows. As Figure 3-10 indicates, there is good agreement in the separation location between the numerical simulations conducted thus far and the corresponding quasi-periodic flow.

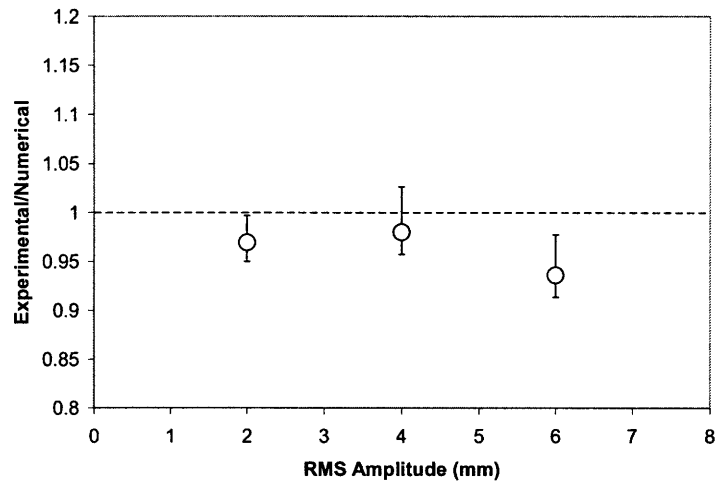


Figure 3-10: Comparison of the separation location results obtained using dye visualization and using numerical simulation of the Haller (2004) criteria.

Chapter 4

Conclusions

Flow separation is an important factor to consider in the design of efficient machines. However, while steady flow separation is a generally well understood concept, a proven and generally accepted understanding of unsteady flow separation does not exist. It was the goal of this study to gain insight into unsteady flow separation in quasi-periodic and aperiodic, two-dimensional flows by investigating the kinematic theory of fixed separation proposed by Haller (2004). By conducting numerical simulations and separation experiments in the rotor-oscillator flow that employed dye visualization, our hope was to be able to reach definitive conclusions about unsteady flow separation.

The flow separation experiments conducted in this study showed that fixed separation does occur in unsteady, quasi-periodic and aperiodic flows. By varying the RMS amplitude of the signals used to drive the unsteady rotor-oscillator flow, we found that larger RMS amplitude motions typically produce separation located further from the center of the cylinder oscillation. This finding can be explained in terms of the skin friction profile along the boundary. Larger RMS amplitudes tend to cause separation further from the center of the cylinder due to the asymmetric skin friction profile that causes the cylinder to ‘push’ the time averaged zero skin friction point away from the center of oscillation. But, a larger RMS amplitude alone does not dictate the separation location. Rather, the nature of the driving signal also affects the separation location in that large variations in the cylinder position do not affect the separation location if the variation occurs on a small enough time scale. This occurs because variation in the cylinder’s motion barely, if at all, affects the time averaged zero skin friction point if the variation occurs

quickly enough. Both this finding and the noted trend between RMS amplitude and separation location qualitatively support the Haller (2004) criteria.

While we have been able to support the Haller (2004) criteria qualitatively, we have not been able to do so quantitatively. Even though preliminary results suggest that the Haller (2004) criteria does indeed successfully predict the location of fixed separation in unsteady, quasi-periodic flows, we cannot definitely make this conclusion since we have yet to compare the measured separation location for all of our generated quasi-periodic flows. Furthermore, as of yet, no work has been completed to investigate the angle of separation in quasi-periodic or aperiodic flows.

Significant work remains before a definitive conclusion can be made about the Haller (2004) criteria. In addition to conducting further experimental and numerical analysis to quantitatively verify the Haller (2004) criteria in predicting both the separation location and angle of separation, we must still prove that the Haller (2004) criteria can be realistically implemented. The ultimate end goal of any project investigating unsteady flow separation is to develop a solid understanding of the dynamics of the physical phenomenon so that it can be harnessed and controlled. But, while an understanding and control criteria are great steps forward, they are utterly useless if one cannot implement them in an effective, efficient, and logical way. Fortunately, the Haller (2004) criteria seems promising, and it is our hope that this study represents a significant step towards fully understanding unsteady flow separation.

Appendix A

Motor control logic

A.1 Motor control logic for quasi-periodic signals

Figures A-1 and A-2 show the LabView wiring diagrams used with quasi-periodic signals to control the motor that was responsible for translating the cylinder.

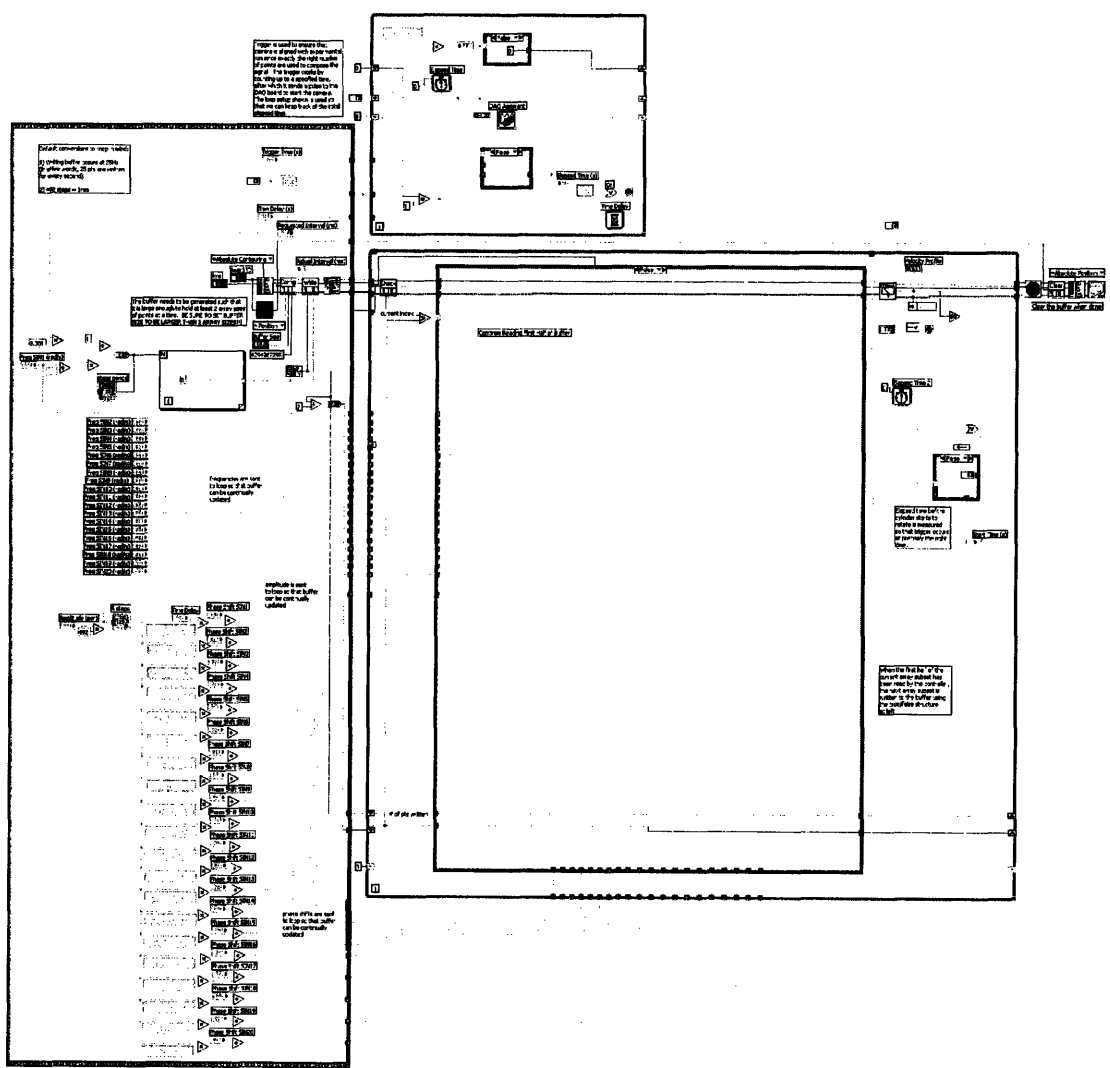


Figure A-1: LabView wiring diagram used with quasi-periodic signals to control the motor that translates the cylinder. The true-false structures are set to false.

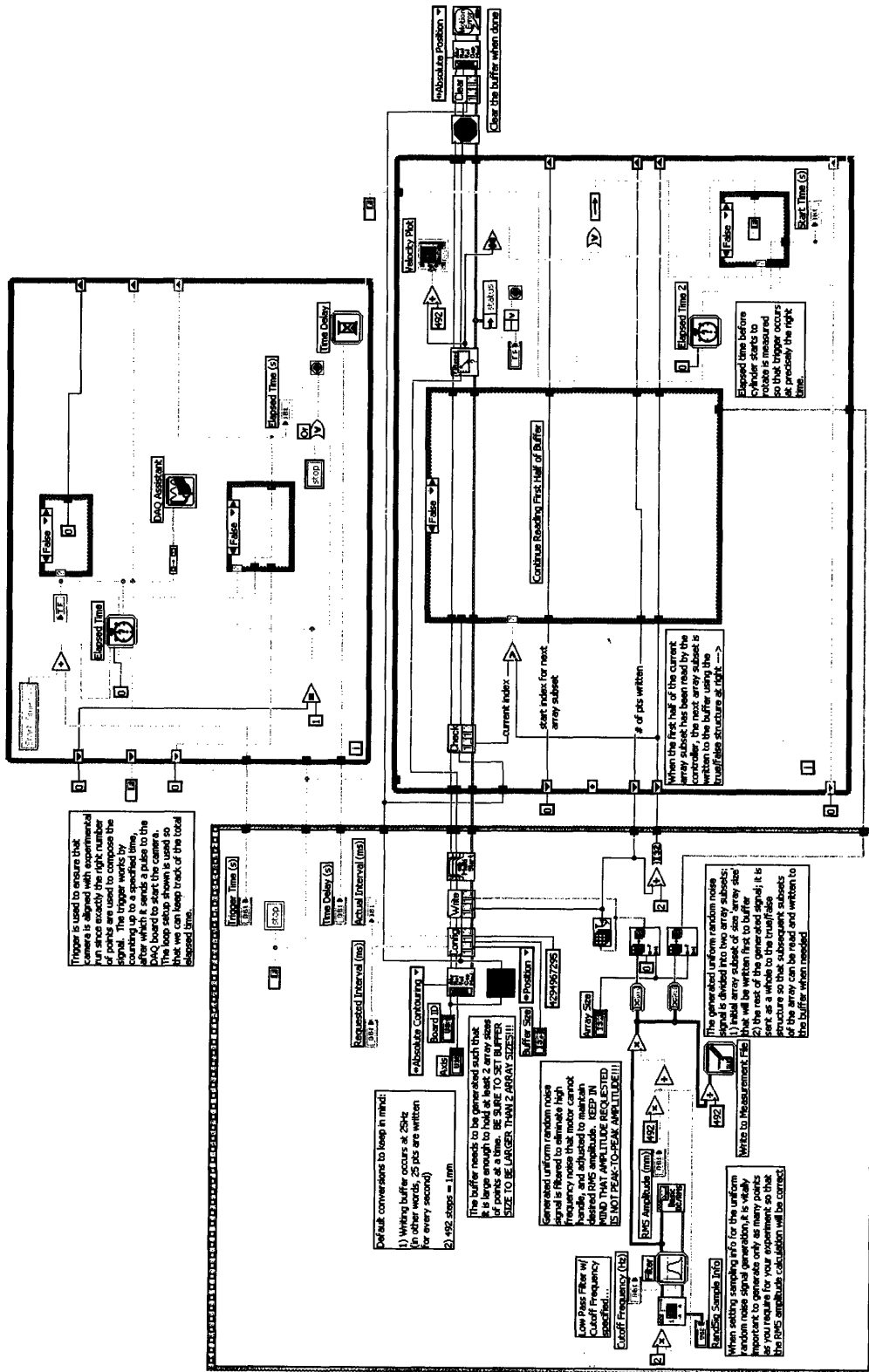


Figure A-3: LabView wiring diagram used when generating aperiodic signals to control the motor that translates the cylinder. The true-false structures are set to false.

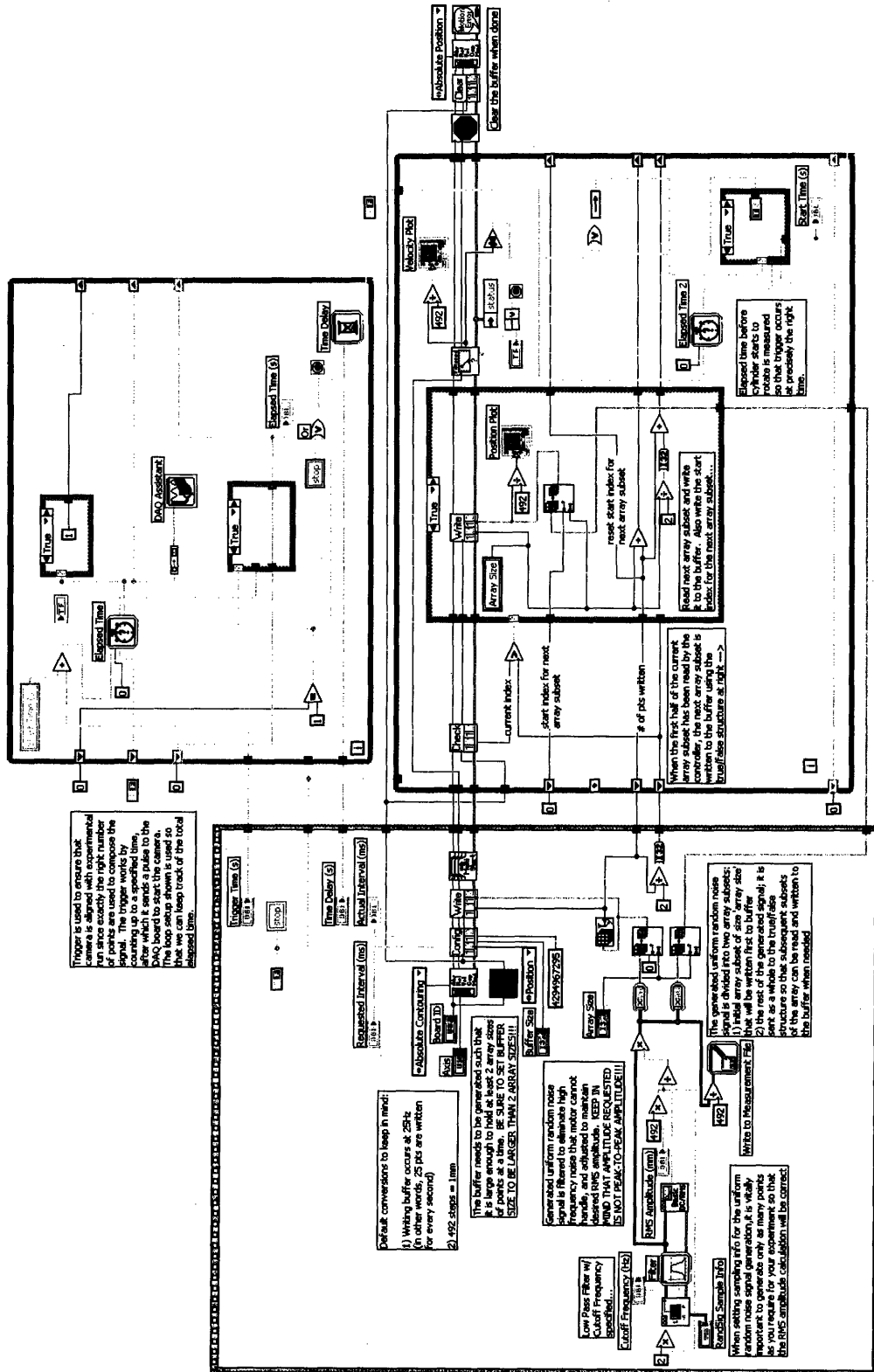


Figure A-4: LabView wiring diagram used when generating aperiodic signals to control the motor that translates the cylinder. The true-false structures are set to true.

Appendix B

Quasi-periodic flow generation

To study fixed separation in unsteady, quasi-periodic flows, two sets of quasi-periodic signals were generated to drive the translational motion of the cylinder (see Section 2.4.1). The first set comprised of six quasi-periodic signals with incommensurate frequencies and phase shifts. The second set comprised of six quasi-periodic signals scaled from the quasi-periodic signal in the first set with RMS amplitude 2.99 mm. Each quasi-periodic signal generated for both sets was of the form described in (2.1) with $N = 20$ sinusoids.

B.1 Generated quasi-periodic signals with incommensurate frequencies and phase shifts

B.1.1 Quasi-periodic signal of RMS amplitude 0.38 mm

Each sinusoidal component of the quasi-periodic signal of RMS amplitude 0.38 mm had an amplitude $a = 0.125$ mm. To ensure that the signal began at the point $(x,y) = (0,0)$, a time shift of +167.9 ms was added to each component. Figure B-1 displays the signal with RMS amplitude 0.38 mm and its autocorrelation while Table B.1 gives the sinusoidal components of the signal.

B.1.2 Quasi-periodic signal of RMS amplitude 0.81 mm

Each sinusoidal component of the quasi-periodic signal of RMS amplitude 0.81 mm had an amplitude $a = 0.25$ mm. To ensure that the signal began at the point $(x,y) = (0,0)$, a time shift of -211.2 ms was added to each component. Figure B-2 displays the signal with RMS amplitude 0.81 mm and its autocorrelation while Table B.2 gives the sinusoidal components of the signal.

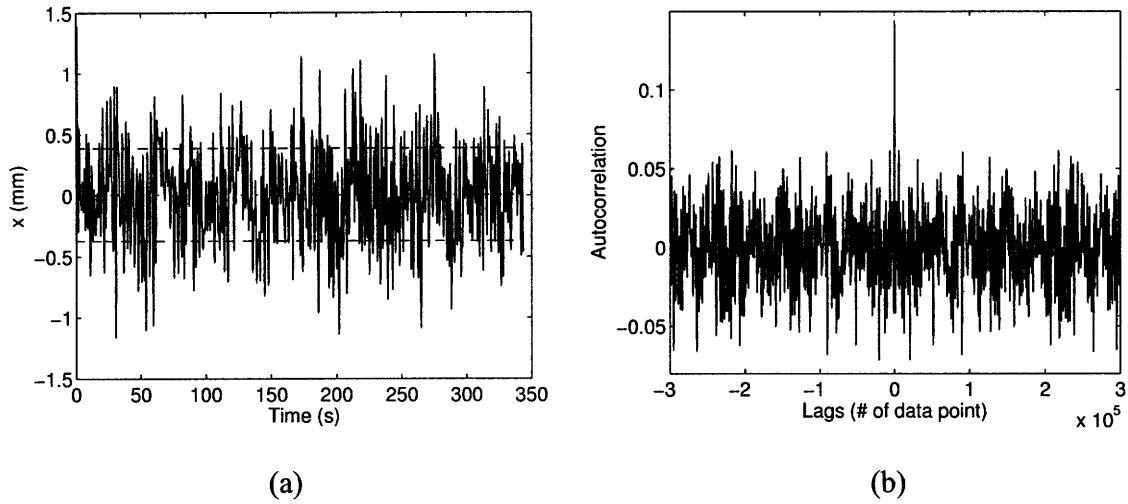


Figure B-1: (a) Quasi-periodic signal of RMS amplitude 0.38 mm used to drive the translational motion of the cylinder, and (b) the autocorrelation of the same signal sampled at 1000 Hz for 343.67 seconds. The mean value and RMS amplitude are shown on the plot of the signal.

Component Number	Frequency (rad/s)	Phase Shift (rad)
1	2.1974	-0.5328
2	1.0113	0.3296
3	0.2077	0.7431
4	2.1394	1.5261
5	4.2921	-1.1237
6	4.0749	-1.5211
7	3.1922	0.7344
8	0.2981	0.9346
9	1.9884	-0.9088
10	3.2252	0.2431
11	3.4630	-1.3108
12	1.6484	-0.9395
13	2.8325	-1.1816
14	2.2262	-1.2391
15	0.1277	-1.4116
16	0.8015	0.0304
17	2.8407	0.0301
18	2.6283	-0.5139
19	3.1736	-1.1999
20	2.2803	1.5556

Table B.1: Frequency and phase shift for each sinusoidal component of the quasi-periodic signal of RMS amplitude 0.38 mm used to drive the translational motion of the cylinder for separation experiments.

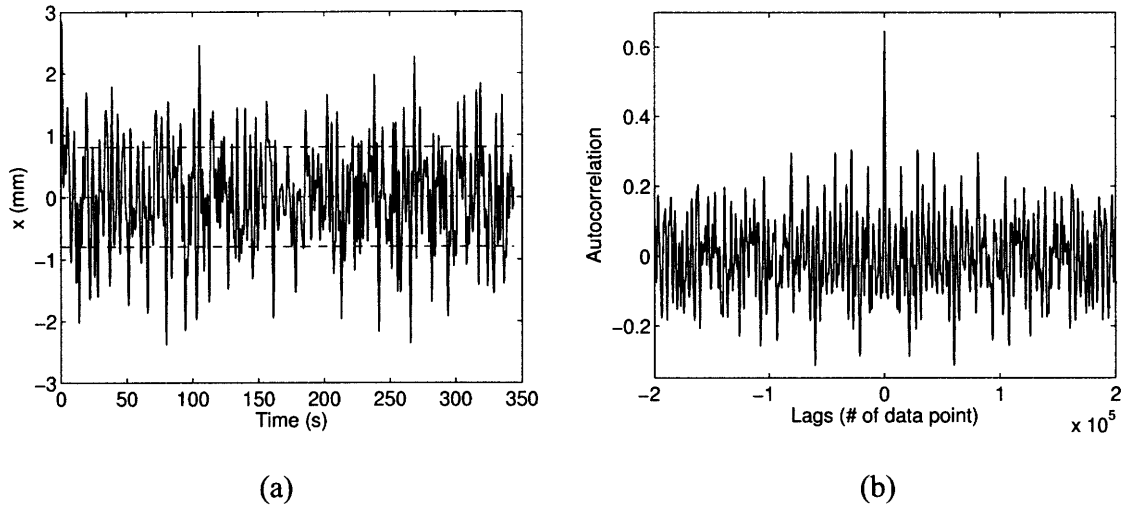


Figure B-2: (a) Quasi-periodic signal of RMS amplitude 0.81 mm used to drive the translational motion of the cylinder, and (b) the autocorrelation of the same signal sampled at 1000 Hz for 343.67 seconds. The mean value and RMS amplitude are shown on the plot of the signal.

Component Number	Frequency (rad/s)	Phase Shift (rad)
1	1.5032	0.3253
2	1.6175	1.4994
3	0.7745	0.5284
4	0.4597	-0.2981
5	0.4451	-0.4893
6	1.7231	-1.4375
7	0.7268	-0.3180
8	0.3782	-0.1802
9	0.1612	1.5603
10	2.1756	0.3614
11	1.9337	1.0359
12	3.0683	-0.1966
13	2.6514	-0.3233
14	1.3171	1.2315
15	1.0830	0.9689
16	3.1153	0.8830
17	2.6689	0.5046
18	0.8526	-0.8142
19	1.3345	0.3065
20	1.3161	0.8405

Table B.2: Frequency and phase shift for each sinusoidal component of the quasi-periodic signal of RMS amplitude 0.81 mm used to drive the translational motion of the cylinder for separation experiments.

B.1.3 Quasi-periodic signal of RMS amplitude 1.54 mm

Each sinusoidal component of the quasi-periodic signal of RMS amplitude 1.54 mm had an amplitude $a = 0.5$ mm. To ensure that the signal began at the point $(x,y) = (0,0)$, a time shift of +1911 ms was added to each component. Figure B-3 displays the signal with RMS amplitude 1.54 mm and its autocorrelation while Table B.3 gives the sinusoidal components of the signal.

B.1.4 Quasi-periodic signal of RMS amplitude 2.36 mm

Each sinusoidal component of the quasi-periodic signal of RMS amplitude 2.36 mm had an amplitude $a = 0.75$ mm. To ensure that the signal began at the point $(x,y) = (0,0)$, a time shift of -73.9 ms was added to each component. Figure B-4 displays the signal with RMS amplitude 2.36 mm and its autocorrelation while Table B.4 gives the sinusoidal components of the signal.

B.1.5 Quasi-periodic signal of RMS amplitude 2.99 mm

Each sinusoidal component of the quasi-periodic signal of RMS amplitude 2.99 mm had an amplitude $a = 1$ mm. To ensure that the signal began at the point $(x,y) = (0,0)$, a time shift of +158.4 ms was added to each component. Figure B-5 displays the signal with RMS amplitude 2.99 mm and its autocorrelation while Table B.5 gives the sinusoidal components of the signal.

B.1.6 Quasi-periodic signal of RMS amplitude 3.83 mm

Each sinusoidal component of the quasi-periodic signal of RMS amplitude 3.83 mm had an amplitude $a = 1.125$ mm. To ensure that the signal began at the point $(x,y) = (0,0)$, a time shift of -5.6 ms was added to each component. Figure B-6 displays the signal with RMS amplitude 3.83 mm and its autocorrelation while Table B.6 gives the sinusoidal components of the signal.

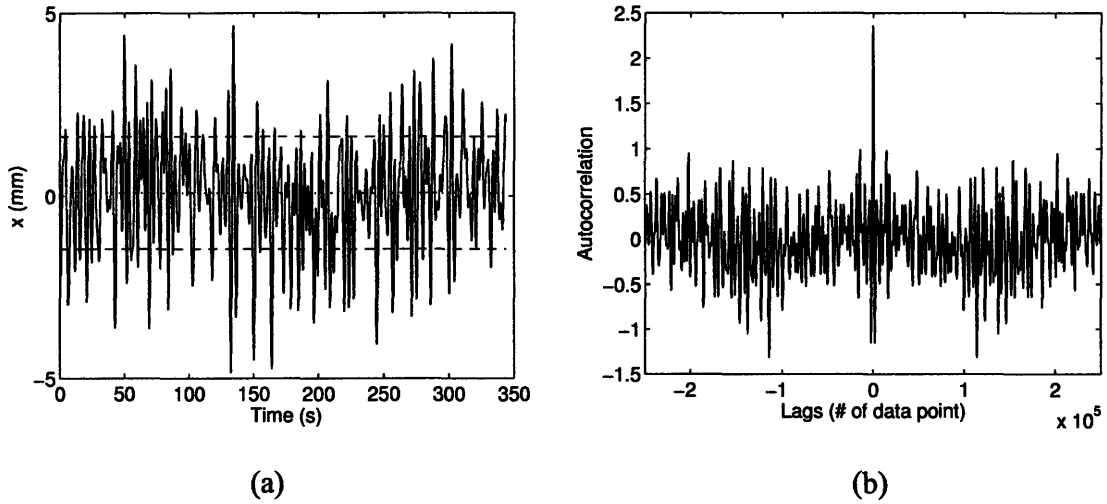


Figure B-3: (a) Quasi-periodic signal of RMS amplitude 1.54 mm used to drive the translational motion of the cylinder, and (b) the autocorrelation of the same signal sampled at 1000 Hz for 343.67 seconds. The mean value and RMS amplitude are shown on the plot of the signal.

Component Number	Frequency (rad/s)	Phase Shift (rad)
1	1.4683	1.2630
2	1.8017	1.0451
3	1.4035	-1.0801
4	1.7177	0.7270
5	1.2386	0.7017
6	0.5258	-0.0319
7	0.9291	0.9289
8	1.6743	-0.8203
9	1.3930	-0.8434
10	1.3509	-0.7273
11	2.1740	0.8178
12	1.0575	1.3986
13	0.7912	-1.3057
14	2.0803	0.5995
15	1.3500	1.2409
16	0.0275	-0.6255
17	2.1167	-1.2501
18	1.3072	-0.0975
19	1.5733	1.1274
20	0.4071	-0.1182

Table B.3: Frequency and phase shift for each sinusoidal component of the quasi-periodic signal of RMS amplitude 1.54 mm used to drive the translational motion of the cylinder for separation experiments.

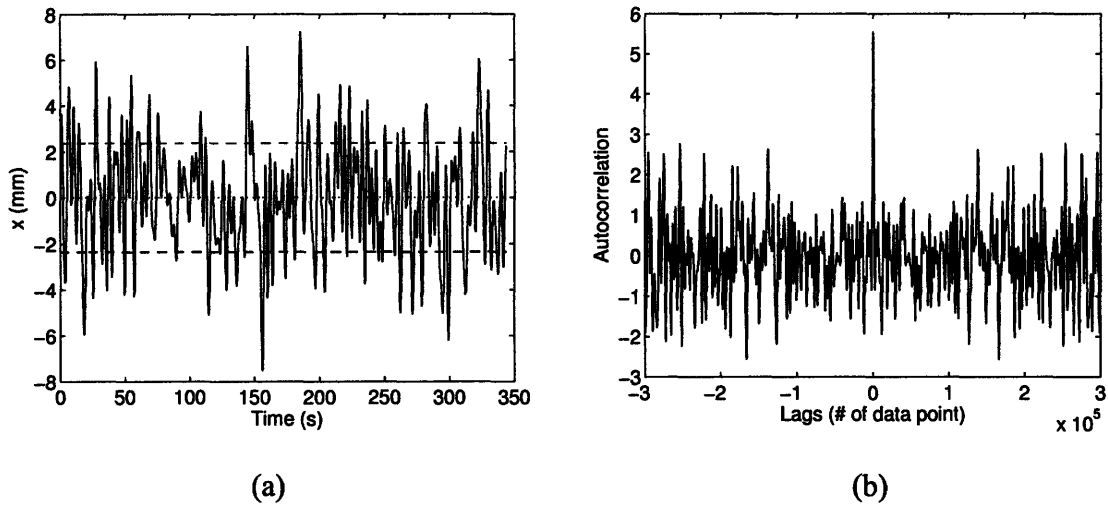


Figure B-4: (a) Quasi-periodic signal of RMS amplitude 2.36 mm used to drive the translational motion of the cylinder, and (b) the autocorrelation of the same signal sampled at 1000 Hz for 343.67 seconds. The mean value and RMS amplitude are shown on the plot of the signal.

Component Number	Frequency (rad/s)	Phase Shift (rad)
1	0.8507	1.4678
2	0.1463	-0.5758
3	0.2779	-1.2070
4	0.3605	-1.2757
5	1.1671	0.8244
6	0.9157	1.0541
7	1.7650	-1.5420
8	1.4140	-1.2178
9	0.4731	1.2858
10	0.3173	-0.9190
11	1.8657	0.6695
12	0.1764	1.0012
13	0.7654	-1.0601
14	1.1838	1.3299
15	0.9587	0.1261
16	1.5317	-1.5643
17	1.8349	1.2234
18	0.0433	-1.2616
19	0.8206	1.4686
20	1.3589	0.5342

Table B.4: Frequency and phase shift for each sinusoidal component of the quasi-periodic signal of RMS amplitude 2.36 mm used to drive the translational motion of the cylinder for separation experiments.

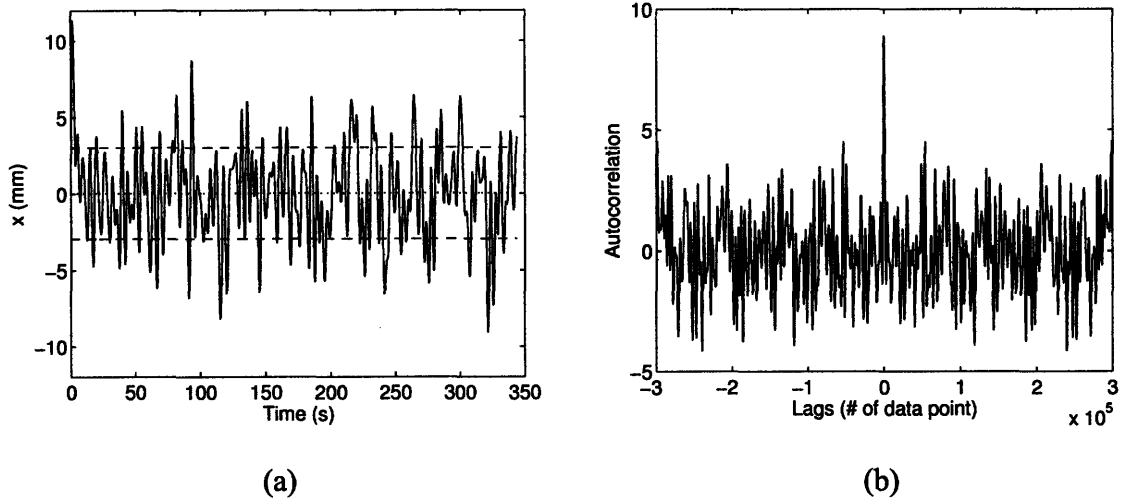


Figure B-5: (a) Quasi-periodic signal of RMS amplitude 2.99 mm used to drive the translational motion of the cylinder, and (b) the autocorrelation of the same signal sampled at 1000 Hz for 343.67 seconds. The mean value and RMS amplitude are shown on the plot of the signal.

Component Number	Frequency (rad/s)	Phase Shift (rad)
1	0.4056	0.6399
2	0.9542	1.3600
3	1.3038	-0.8544
4	0.8218	-1.0298
5	1.7707	-0.4533
6	0.0896	0.8022
7	1.6355	-0.6718
8	0.4591	1.3595
9	0.2394	1.3849
10	1.2828	1.0923
11	0.3825	-0.1411
12	0.1482	1.1031
13	1.0273	-0.5677
14	0.6852	1.1555
15	0.6802	-1.3393
16	0.3652	-1.4153
17	1.0358	-1.1878
18	0.9543	-1.2030
19	1.4072	-0.3925
20	1.5049	-1.4243

Table B.5: Frequency and phase shift for each sinusoidal component of the quasi-periodic signal of RMS amplitude 2.99 mm used to drive the translational motion of the cylinder for separation experiments.

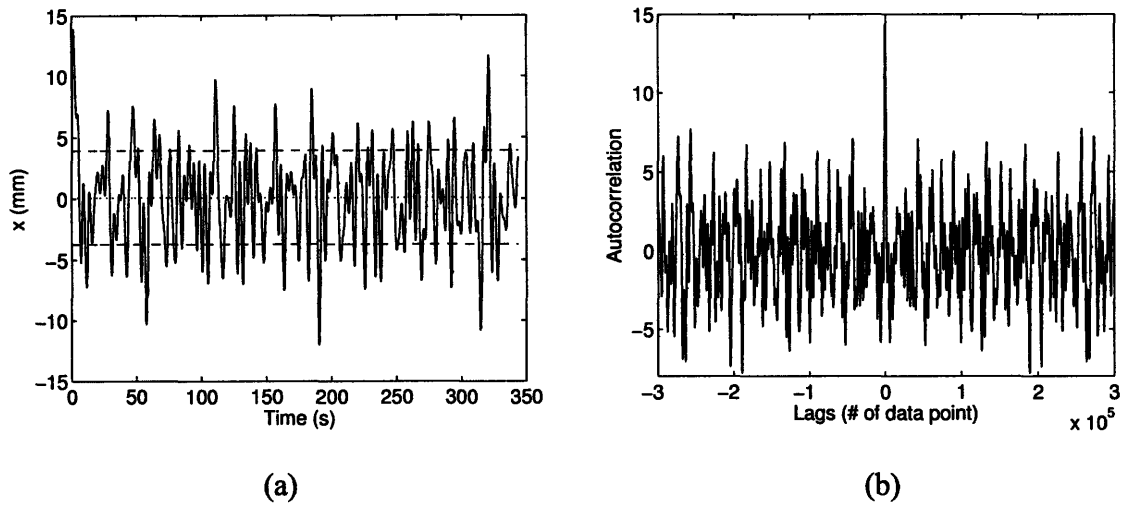


Figure B-6: (a) Quasi-periodic signal of RMS amplitude 3.83 mm used to drive the translational motion of the cylinder, and (b) the autocorrelation of the same signal sampled at 1000 Hz for 343.67 seconds. The mean value and RMS amplitude are shown on the plot of the signal.

Component Number	Frequency (rad/s)	Phase Shift (rad)
1	1.3701	0.3459
2	1.1835	-1.2812
3	0.7168	-0.3909
4	0.2803	1.0466
5	1.4149	-0.1520
6	1.6139	-1.1085
7	1.4677	0.8465
8	0.7494	0.3789
9	1.6056	0.4399
10	0.4173	-0.4628
11	0.3169	-0.0294
12	0.6905	-0.1146
13	1.0307	-1.3472
14	0.5302	0.3405
15	0.2953	0.3802
16	0.4150	0.2744
17	0.8538	-0.1107
18	0.9134	1.3896
19	0.5766	-0.3085
20	0.5191	-0.2778

Table B.6: Frequency and phase shift for each sinusoidal component of the quasi-periodic signal of RMS amplitude 3.83 mm used to drive the translational motion of the cylinder for separation experiments.

B.2 Generated quasi-periodic signals with equal frequencies and phase shifts

Because each of the six signals that comprised the second set of quasi-periodic signals employed in our separation experiments were scaled from the quasi-periodic signal in the first set with RMS amplitude 2.99 mm (see Appendix B.1.5), each is essentially identical to the signal presented in Appendix B.1.5 except in amplitude. Table B.7 gives the amplitudes used with the signal presented in Appendix B.1.5 to attain the set of quasi-periodic signals with equal frequencies and phase shifts:

RMS Amplitude of Signal (mm)	Amplitude of each Sinusoid Component of Signal (mm)
2	0.67
2.99	1.00
4	1.34
6	2.01
8	2.68
10	3.35

Table B.7: Required amplitude for each sinusoidal component of the signal described in Appendix B.1.5 necessary to produce specified RMS amplitude of signal.

Appendix C

Aperiodic flow generation

To study fixed separation in unsteady, aperiodic flows, the LabView software package version 7.0 was used to generate a random signal at a specified RMS amplitude to drive the translational motion of the cylinder (see Section 2.4.2). Specifically, random signals with RMS amplitudes that corresponded to the six scaled quasi-periodic signals discussed in Section 3.1.1 and Appendix B.2 were investigated.

C.1 Generated random signals

C.1.1 Random signal of RMS amplitude 2 mm

Figure C-1 shows the random signal of RMS amplitude 2 mm that was used to drive the translational motion of the cylinder, as well as its autocorrelation. The flow generated by this signal was compared to the flow generated by the signal of equal RMS amplitude presented in Appendix B.2.

C.1.2 Random signal of RMS amplitude 2.99 mm

Figure C-2 shows the random signal of RMS amplitude 2.99 mm that was used to drive the translational motion of the cylinder, as well as its autocorrelation. The flow generated by this signal was compared to the flow generated by the signal of equal RMS amplitude presented in Appendix B.2.

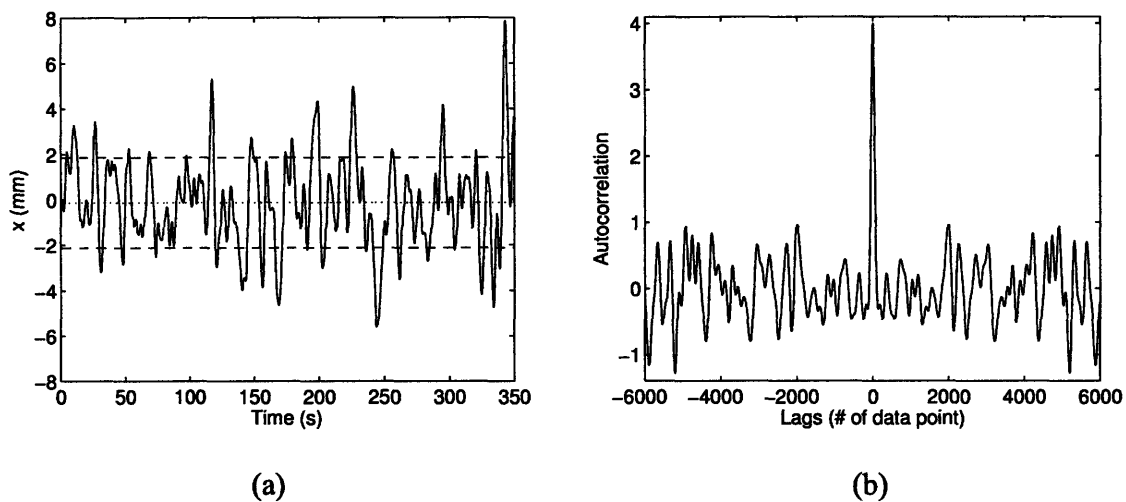


Figure C-1: (a) Random signal of RMS amplitude 2 mm used to drive the translational motion of the cylinder, and (b) the autocorrelation of the same signal sampled at 25 Hz for 350 seconds. The mean value and RMS amplitude are shown on the plot of the signal.

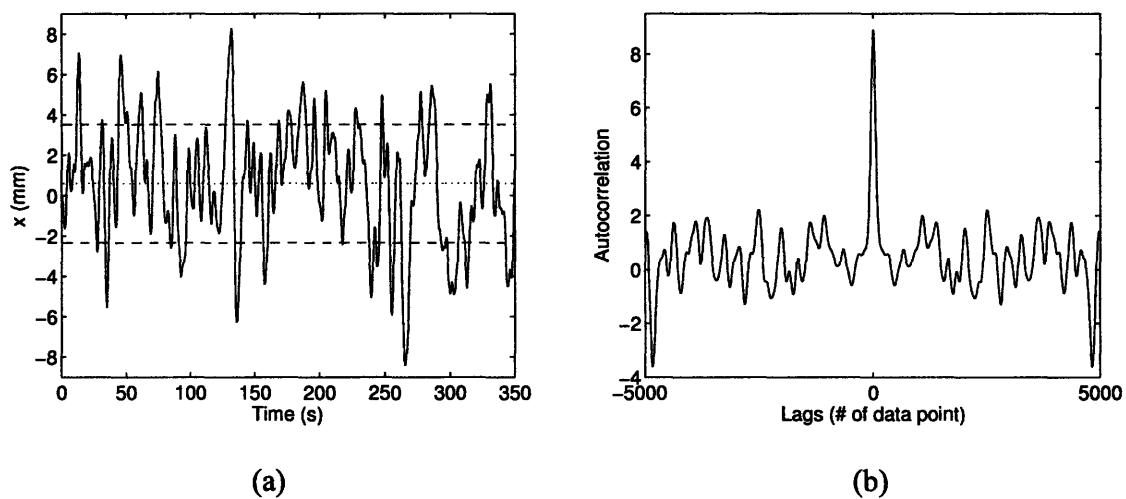


Figure C-2: (a) Random signal of RMS amplitude 2.99 mm used to drive the translational motion of the cylinder, and (b) the autocorrelation of the same signal sampled at 25 Hz for 350 seconds. The mean value and RMS amplitude are shown on the plot of the signal.

C.1.3 Random signal of RMS amplitude 4 mm

Figure C-3 shows the random signal of RMS amplitude 4 mm that was used to drive the translational motion of the cylinder, as well as its autocorrelation. The flow generated by this signal was compared to the flow generated by the signal of equal RMS amplitude presented in Appendix B.2. Another random signal of RMS amplitude 4 mm was used to verify our results. This signal and its autocorrelation are given in Figure C-4.

C.1.4 Random signal of RMS amplitude 6 mm

Figure C-5 shows the random signal of RMS amplitude 6 mm that was used to drive the translational motion of the cylinder, as well as its autocorrelation. The flow generated by this signal was compared to the flow generated by the signal of equal RMS amplitude presented in Appendix B.2. Again, another random signal of RMS amplitude 6 mm was used to verify our results. This signal and its autocorrelation are given in Figure C-6.

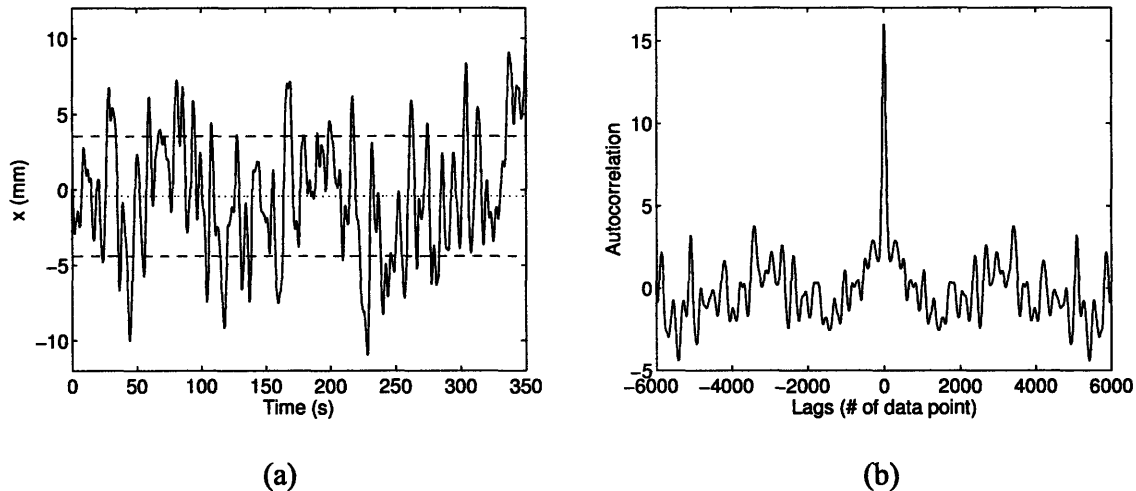
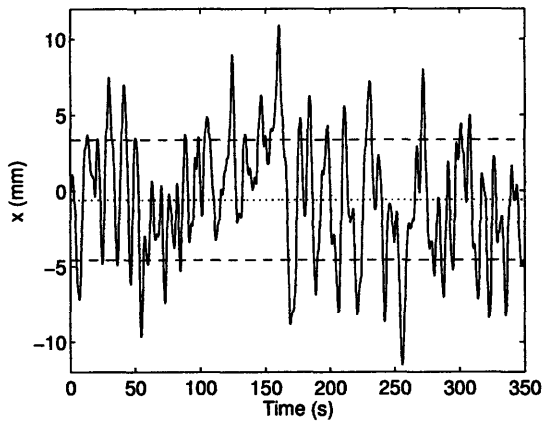
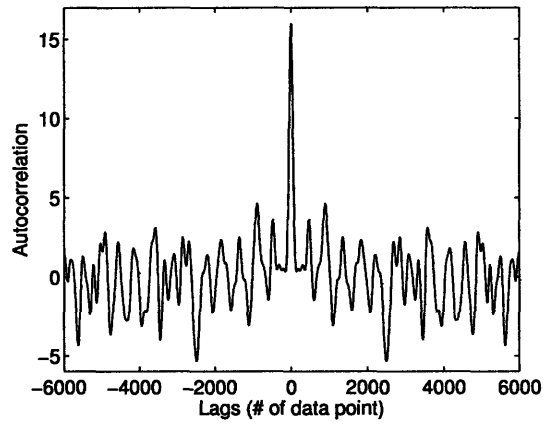


Figure C-3: (a) Random signal of RMS amplitude 4 mm used to drive the translational motion of the cylinder, and (b) the autocorrelation of the same signal sampled at 25 Hz for 350 seconds. The mean value and RMS amplitude are shown on the plot of the signal.

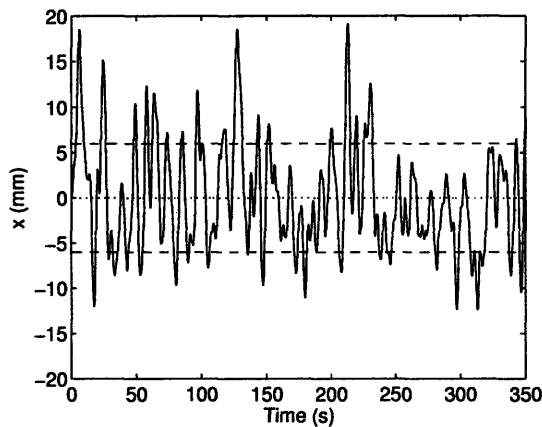


(a)

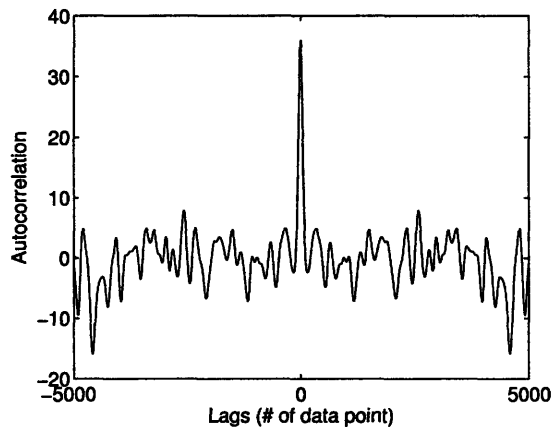


(b)

Figure C-4: (a) Random signal of RMS amplitude 4 mm used to drive the translational motion of the cylinder to verify the results of the separation experiment conducted using the signal shown in Figure C-3, and (b) the autocorrelation of the same signal sampled at 25 Hz for 350 seconds. The mean value and RMS amplitude are shown on the plot of the signal.



(a)



(b)

Figure C-5: (a) Random signal of RMS amplitude 6 mm used to drive the translational motion of the cylinder, and (b) the autocorrelation of the same signal sampled at 25 Hz for 350 seconds. The mean value and RMS amplitude are shown on the plot of the signal.

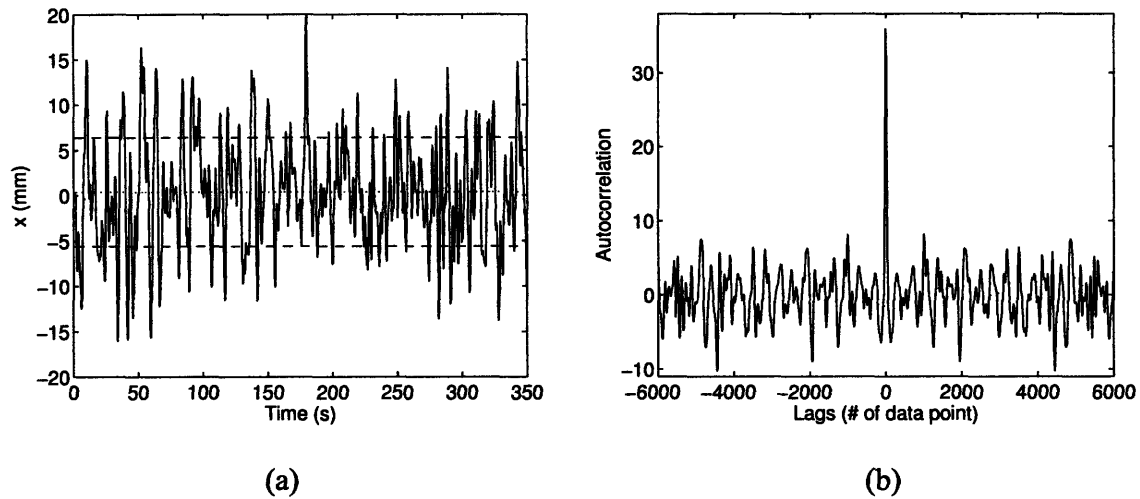


Figure C-6: (a) Random signal of RMS amplitude 6 mm used to drive the translational motion of the cylinder to verify the results of the separation experiment conducted using the signal shown in Figure C-5, and (b) the autocorrelation of the same signal sampled at 25 Hz for 350 seconds. The mean value and RMS amplitude are shown on the plot of the signal.

C.1.5 Random signal of RMS amplitude 8 mm

Figure C-7 shows the random signal of RMS amplitude 8 mm that was used to drive the translational motion of the cylinder, as well as its autocorrelation. The flow generated by this signal was compared to the flow generated by the signal of equal RMS amplitude presented in Appendix B.2. Another random signal of RMS amplitude 8 mm was used to verify our results also. This signal and its autocorrelation are given in Figure C-8.

C.1.6 Random signal of RMS amplitude 10 mm

Figure C-9 shows the random signal of RMS amplitude 10 mm that was used to drive the translational motion of the cylinder, as well as its autocorrelation. The flow generated by this signal was compared to the flow generated by the signal of equal RMS amplitude presented in Appendix B.2.

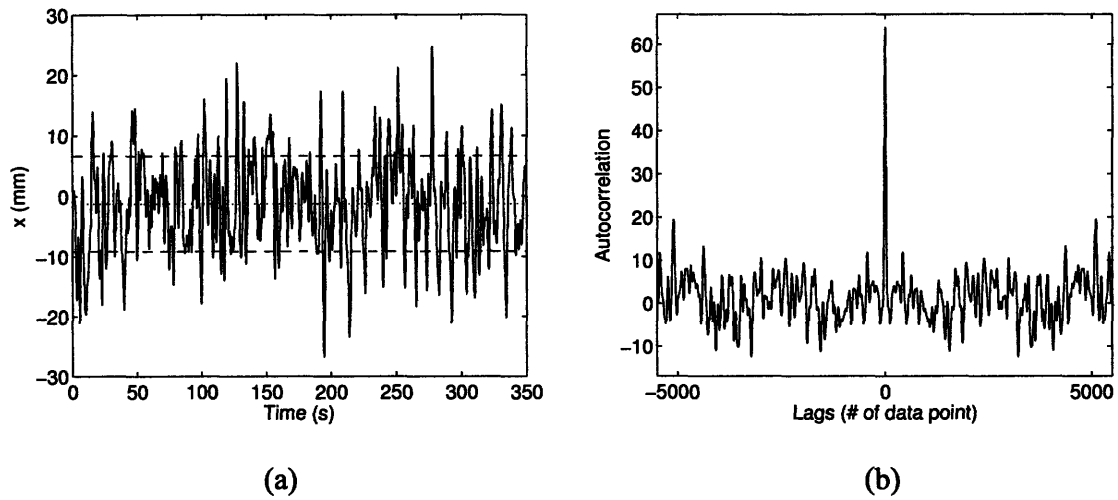


Figure C-7: (a) Random signal of RMS amplitude 8 mm used to drive the translational motion of the cylinder, and (b) the autocorrelation of the same signal sampled at 25 Hz for 350 seconds. The mean value and RMS amplitude are shown on the plot of the signal.

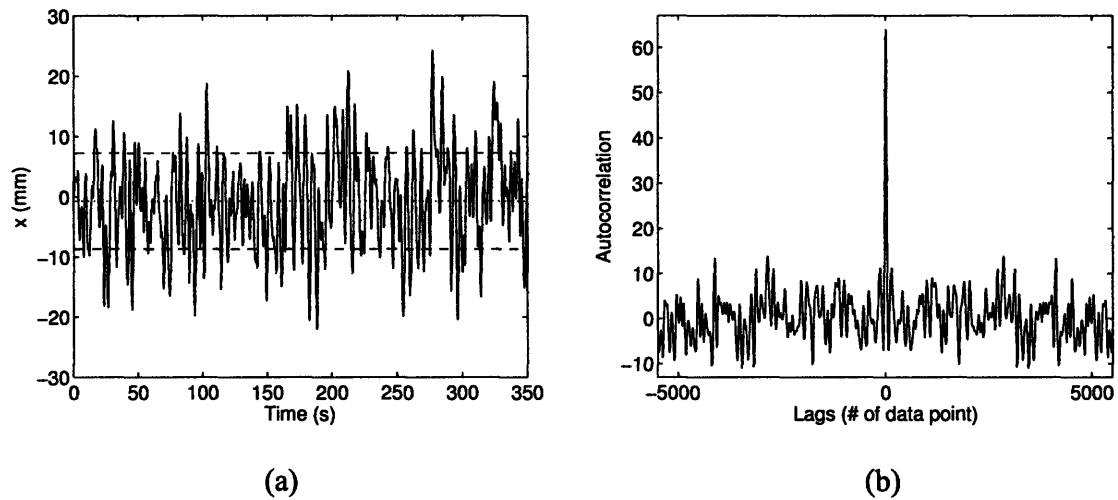
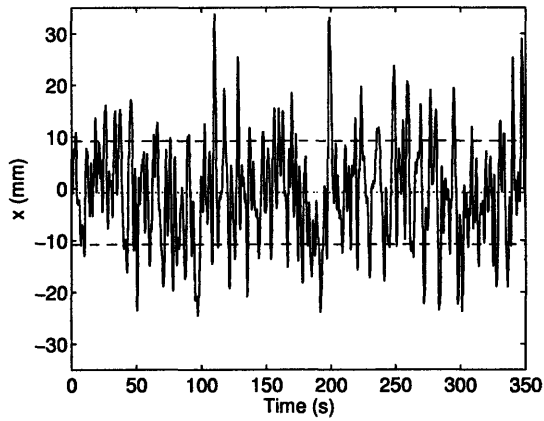
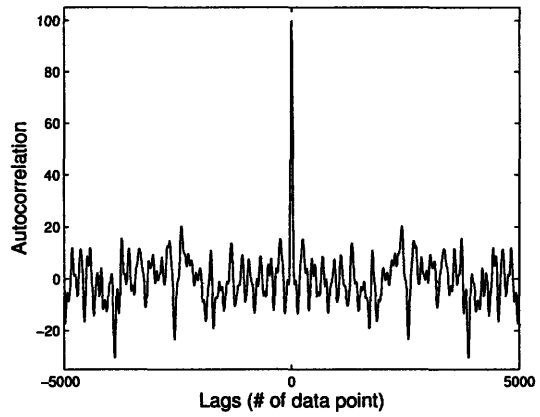


Figure C-8: (a) Random signal of RMS amplitude 8 mm used to drive the translational motion of the cylinder to verify the results of the separation experiment conducted using the signal shown in Figure C-7, and (b) the autocorrelation of the same signal sampled at 25 Hz for 350 seconds. The mean value and RMS amplitude are shown on the plot of the signal.



(a)



(b)

Figure C-9: (a) Random signal of RMS amplitude 10 mm used to drive the translational motion of the cylinder, and (b) the autocorrelation of the same signal sampled at 25 Hz for 350 seconds. The mean value and RMS amplitude are shown on the plot of the signal.

References

- [1] FUMAGALLI, M. 2002 *A numerical investigation of particle motion and deposition on a cross oscillating cylinder*. MS thesis, University of Illinois at Chicago. Chicago, IL.
- [2] HACKBORN, W. W., ULUCAKLI, M. E., & YUSTER, T. 1997 A theoretical and experimental study of hyperbolic and degenerative mixing regions in a chaotic Stokes flow. *J. Fluid Mech.* 346, pp. 23-48.
- [3] HALLER, G. 2004 Exact theory of unsteady separation for two-dimensional flows. *J. Fluid Mech.* 512, pp. 257-311.
- [4] LIGHTHILL, M. J. 1963 Boundary layer theory. In *Laminar Boundary Layers* (ed. L. Rosenhead). Dover.
- [5] LIU, C. S. & WAN, Y. H. 1985 A simple exact solution of the Prandtl boundary layer equations containing a point of separation. *Arch. Rat. Mech. Anal.* 89, pp. 177-185.
- [6] MOFFATT, H. K. 1964 Viscous and resistive eddies near a sharp corner. *J. Fluid Mech.* 18, 1.
- [7] MOORE, F. K. 1958 On the separation of unsteady boundary layer. In *Boundary-layer Research* (ed. H. Görtler) pp. 296-311. Springer.
- [8] PRANDTL, L. 1904 Über Flüssigkeitsbewegung bei sehr kleiner Reibung. *Verh. III, Int. Math. Kongr., Heidelberg* pp. 484-491.
- [9] ROTT, N. 1956 Unsteady viscous flows in the vicinity of a separation point. *Q. Appl. Maths* 13, pp. 444-451.
- [10] SEARS, W. R. & TELLIONIS, D. P. 1971 Unsteady boundary layer separation. In *Recent Research on Unsteady Boundary Layers* (ed. E. Eichelbrenner), pp. 404-447.

- [11] SEARS, W. R. & TELLIONIS, D. P. 1975 Boundary-layer separation in unsteady flow. *SIAM J. Appl. Maths* 28, pp. 215-235.
- [12] SHARIFF, K., PULLIAM, T. H., & OTTINO, J. M. 1991 A dynamical systems analysis of kinematics in the time-periodic wake of a circular cylinder. *Lect. Appl. Math.* 28, pp. 613-646.
- [13] VAN DOMMELEN, L. L. 1981 *Unsteady Boundary Layer Separation*. PhD thesis, Cornell University. Ithaca, NY.
- [14] VAN DOMMELEN, L. L. & SHEN, S. F. 1982 The genesis of separation. In *Numerical and Physical Aspects of Aerodynamics Flow* (ed. T. Cebici) pp. 283-311. Long Beach, California.
- [15] WILLIAMS, J. C. 1977 Incompressible boundary layer separation. *Annu. Rev. Fluid. Mech.* 9, 113-144.
- [16] WU, J. Z., TRAMEL, R. W., ZHU, F. L. & YIN, X. Y. 2000 A vorticity dynamics theory of three-dimensional flow separation. *Phys. Fluids A* 12, pp. 1932-1954.
- [17] YOUNG, A. D. & HORTON, H. P. 1966 Some results of investigation of separation bubbles. *AGARD CP* No. 4, pp. 779-811.
- [18] YUSTER, T. & HACKBORN, W. W. 1997 On invariant manifolds attached to oscillating boundaries of Stokes flows. *Chaos* 7, pp. 769-776.